European Journal of Taxonomy 947: 20–52
https://doi.org/10.5852/ejt.2024.947.2619
ISSN 2118-9773
www.europeanjournaloftaxonomy.eu
2024 · Tumanov D.V. *et al.*

Research article

urn:lsid:zoobank.org:pub:5B9DA044-2842-456C-8339-2D097A24A662

Integrative description of two new species of the genus *Mesobiotus* (Eutardigrada, Macrobiotoidea) from Russia, with an updated phylogeny of the genus

Denis V. TUMANOV [1,*], Evgenia D. ANDROSOVA [2], Marina D. GAVRILENKO [3] & Aidar A. KALIMULLIN [4]

[1] Department of Invertebrate Zoology, Faculty of Biology, Saint Petersburg State University, 199034, Universitetskaya nab. 7/9, Saint Petersburg, Russia.
[1] Marine Research Laboratory, Zoological Institute of the Russian Academy of Sciences, 199034, Universitetskaja nab. 1, Saint Petersburg, Russia.
[2] Soil Science & Soil Ecology Department, Institute of Earth Sciences, Saint Petersburg State University, 16 Linija, 29, Saint Petersburg, 199178, Russia.
[3] Department of Genetics and Biotechnology, Faculty of Biology, Saint Petersburg State University, 199034, Universitetskaya nab. 7/9, Saint Petersburg, Russia.
[4] Department of Invertebrate Zoology, Faculty of Biology, Far Eastern Federal University, 10 Ajax Bay, Russky Island, Vladivostok, 690922, Russia.

[*] Corresponding author: d.tumanov@spbu.ru
[2] Email: eugenia.androsova@gmail.com
[3] Email: md.gavrilenko7@gmail.com
[4] Email: kalimullin.aa@students.dvfu.ru

[1] urn:lsid:zoobank.org:author:49E22A70-C27B-485B-941E-577666EE65F9
[2] urn:lsid:zoobank.org:author:73698C49-9E5B-48F0-A271-03886446FF08
[3] urn:lsid:zoobank.org:author:63202CD2-E90E-482C-B2DF-92A354821CDE
[4] urn:lsid:zoobank.org:author:641F4F4E-D6FD-423B-B683-04ABDB4628F3

Abstract. In this study, we describe two new species of *Mesobiotus* based on morphological data collected through light and scanning electron microscopy. Descriptions include DNA sequences of four commonly used molecular markers (18S rDNA, 28S rDNA, ITS-2, and COI). *Mesobiotus efa* sp. nov. was discovered in North-West Russia and belongs to the group of species with smooth cuticle, *harmsworthi*-type OCA, typical *Mesobiotus* claws IV with unindented lunules, and egg chorion with reticulated processes in form of 'sharp wide cones' or 'cones with long slender endings', egg process bases with well-developed crone of dark thickenings without finger-like projections, and egg shell surface between the processes with ridges without reticulation, areolation or semi-areolation. It can be distinguished from all know species of this group by a unique combination of morphological and morphometric characters. *Mesobiotus vulpinus* sp. nov. was found in the Russian Far East, and is similar to *Mesobiotus mauccii* by having an egg chorion with polygonal relief. The new species can be distinguished from *M. mauccii* by having a narrower buccal tube, by details of oral cavity armature, and by longer egg chorion processes. Furthermore, we provide results of the phylogenetic analyses of the genus *Mesobiotus* conducted in this study.

Keywords. Egg ornamentation, morphology, *Mesobiotus mauccii*, new species, tardigrades, Macrobiotidae, Far East, North-West.

Tumanov D.V., Androsova E,D., Gavrilenko M.D. & Kalimullin A.A. 2024. Integrative description of two new species of the genus *Mesobiotus* (Eutardigrada, Macrobiotoidea) from Russia, with an updated phylogeny of the genus. *European Journal of Taxonomy* 947: 20–52. https://doi.org/10.5852/ejt.2024.947.2619

Introduction

Tardigrades are a group of microscopic segmented animals widely distributed in the nature (Nelson 2018). Despite its strictly aquatic lifestyle this group successfully invaded terrestrial ecotopes being associated with habitats that periodically contains liquid water – moss cushions, lichens, soil, and leaf debris (Nelson 2018). Semiterrestrial tardigrades (tardigrades that live in terrestrial habitats subjected to periodic desiccation) comprise most of the species diversity of this group.

Macrobiotidae Thulin, 1928 is the largest Eutardigrada Richters, 1926 family which includes four most species-rich genera of semiterrestrial eutardigrades: *Macrobiotus* Schultze, 1834, *Mesobiotus* Vecchi, Cesari, Bertolani, Jönsson, Rebecchi & Guidetti, 2016, *Minibiotus* Schuster, 1980, and *Paramacrobiotus* Guidetti, Schill, Bertolani, Dandekar & Wolf, 2009. All these genera are the subjects of intensive study, with numerous new species descriptions, taxonomic revisions and phylogenetic reconstructions (Kaczmarek & Michalczyk 2017; Kaczmarek *et al.* 2017, 2018, 2020, 2023; Guidetti *et al.* 2019; Stec *et al.* 2020a, 2020b, 2021a, 2021b, 2022; Tumanov 2020a; Short *et al.* 2022; Stec 2022; Bertolani *et al.* 2023; Vecchi *et al.* 2023).

The genus *Mesobiotus* with 76 currently described species (Degma & Guidetti 2023; Vecchi *et al.* 2023) is a second large genus within Macrobiotidae. Modern integrative redescription of its type species *Mesobiotus harmsworthi* (Murray, 1907) given by Kaczmarek *et al.* (2018) together with the revisions of the genus morphology and phylogeny (Kaczmarek *et al.* 2020; Stec 2022) provided a strong base for the description of new species of *Mesobiotus*.

Fauna of semiterrestrial tardigrades of Russia is poorly investigated (see Tumanov *et al.* 2022). All records of species of *Mesobiotus* for this territory originates from the publications that precede the modern revision of the Macrobiotidae taxonomy and should be considered dubious except for *Mesobiotus montanus* (Murray, 1910) noted for several regions of northern Russia (Biserov 1991, 1996), and *Mesobiotus altitudinalis* (Biserov, 1997–1998) described from North Ossetia. Biserov (1991) noted *Mesobiotus furciger* (Murray, 1907, as *Macrobiotus*) for Udmurtia. In our opinion, this record should be attributed as belonging to the unknown species of the polyphyletic *Mesobiotus furciger* morpho-group (according to Stec 2022). Numerous records of *M. harmsworthi*, *M. harmsworthi coronatus*, and *M. harmsworthi obscurus* are not valid due to changes in *Mesobiotus* taxonomy that have taken place since their publication (Pilato *et al.* 2000; Kaczmarek *et al.* 2018, 2020; Stec 2022).

In this paper, we describe two new species of *Mesobiotus* which have been found during the investigation of the tardigrade fauna of Russia. The detailed morphological description is supplemented by DNA sequences of four standard genes used in tardigrade taxonomy and phylogenetics (the nuclear 18S rRNA, 28S rRNA, ITS-2, and the mitochondrial COI). We also performed a multigene phylogenetic analysis in order to determine the position of new species on the *Mesobiotus* phylogenetic tree and to reconstruct an updated phylogeny of the genus.

Material and methods

Sampling

The moss samples were collected in the vicinity of the cities of St Petersburg and Vladivostok. Material was stored within paper envelopes at room temperature. Tardigrade specimens were extracted from rehydrated samples using the standard technique of washing them through two sieves (first with ≈ 1 mm mesh size and second with 29 μm mesh size; Tumanov 2018a). The contents of the finer sieve were examined under a Leica M205C stereo microscope.

Microscopy and imaging

Tardigrades found were fixed with acetic acid or relaxed by incubating live individuals at 60°C for 30 min (Morek *et al.* 2016) and mounted on slides in Hoyer's medium. Permanent slides were examined under a Leica DM2500 microscope equipped with phase contrast (PhC) and differential interference contrast (DIC). Photographs were taken using a Nikon DS-Fi3 digital camera with NIS software.

For scanning electron microscopy (SEM) specimens were thermally relaxed at 60°C (Morek *et al.* 2016), dehydrated in an ascending ethyl alcohol series (10%, 20%, 30%, 50%, 70%, 96%), transferred to 100% acetone, critical-point dried in CO_2, mounted on stubs and coated with gold. A Tescan MIRA3 LMU Scanning Electron Microscope was used for observations (Centre for Molecular and Cell Technologies, St Petersburg State University).

Morphometrics and terminology

The sample size for morphometrics was chosen following the recommendations of Stec *et al.* (2016). Structures were measured only if their orientations were suitable. Body length was measured from the anterior end of the body to the posterior end, excluding the hind legs. The buccal tube was measured from the dorsal crests of the oral cavity armature (OCA) to the caudal end of the buccal tube, not including the buccal apophyses. Terminology for the structures within the bucco-pharyngeal apparatus and for the claws follows those of Michalczyk & Kaczmarek (2003) and Pilato & Binda (2010). Elements of the buccal apparatus, claws and eggs were measured according to Kaczmarek & Michalczyk (2017). The macroplacoid length sequence is given according to Kaczmarek *et al.* (2014). Cuticular structures under claws on legs I–III are described according to Kiosya *et al.* (2021). All measurements are given in micrometres (μm). The pt index used is the percentage ratio between the length of a structure and the length of the buccal tube (Pilato 1981), and is presented here in italics. Morphometric data were handled using ver. 1.6 of the "Parachela" template, which is available from the Tardigrada Register (Michalczyk & Kaczmarek 2013).

Genotyping

DNA was extracted from individual specimens using QuickExtract™ DNA Extraction Solution (Lucigen Corporation, USA; see description of complete protocol in Tumanov 2020b). Preserved exoskeletons were recovered, mounted on a microscope slide in Hoyer's medium and retained as the hologenophore (Pleijel *et al.* 2008).

Four genes were sequenced: a small ribosome subunit (18S rRNA) gene, a large ribosome subunit (28S rRNA) gene, internal transcribed spacer (ITS-2), and the cytochrome oxidase subunit I (COI) gene. PCR reactions included 5 μl template DNA, 1 μl of each primer, 1 μl DNTP, 5 μl Taq Buffer (10×) (−Mg), 4 μl 25 mM $MgCl_2$ and 0.2 μl Taq DNA Polymerase (Thermo Scientific™) in a final volume of 50 μl. The primers and PCR programs used are listed in electronic supplementary material (see Supp. file 1). The PCR products were visualised in 1.5% agarose gel stained with ethidium bromide. All amplicons were sequenced directly using the ABI PRISM Big Dye Terminator Cycle Sequencing Kit (Applied Biosystems, Foster City, CA, USA) with the help of an ABI Prism 310 Genetic Analyzer in the

Core Facilities Center "Centre for Molecular and Cell Technologies" of St Petersburg State University. Sequences were edited and assembled using ChromasPro software (Technelysium, USA). The COI sequences were translated to amino acids using the invertebrate mitochondrial code, MEGA11 (Tamura *et al.* 2021), in order to check for the presence of stop codons and therefore of pseudogenes. Uncorrected pairwise distances were calculated using MEGA11 with gaps/missing data treatment set to "pairwise deletion". All obtained sequences were deposited in GenBank (https://www.ncbi.nlm.nih.gov/genbank/ – accession numbers available in the species descriptions).

Phylogenetic analyses

Sequences of 18S, 28S, ITS-2, and COI markers representing all species of *Mesobiotus* for which at least two of the abovementioned markers were available in GenBank at the time of the analysis were downloaded. Sequences of appropriate length that were homologous to the sequences obtained and originated from publications with a reliable attribution of the investigated taxa were selected, with addition of the newly obtained sequences (Table 1). *Richtersius coronifer* (Richters, 1903) (Macrobiotoidea, Richtersiusidae) was used as an outgroup.

Sequences were automatically aligned with the MAFFT algorithm (Katoh *et al.* 2002) with the software AliView ver. 1.27 (Larsson 2014); the alignments were cropped to a length of 983 bp for 18S, 770 bp for 28S, 566 bp for ITS-2, and 657 bp for COI. Sequences of all genes were concatenated using SeaView ver. 4.0 (Gouy *et al.* 2010) (final alignment presented in Supp. file 2). Maximum-likelihood (ML) topologies were constructed using IQ-TREE software multicore ver. 1.6.12 (Kalyaanamoorthy *et al.* 2017; Minh *et al.* 2020). The best substitution model and partitioning scheme for posterior phylogenetic analysis was automatically chosen by IQ-TREE software for each of 6 partitions (18S/28S/ITS-2/COI 1-2-3 codon positions) (see Supp. file 3). Bayesian analysis of the same datasets was performed using MrBayes ver. 3.2.6, GTR model with gamma correction for intersite rate variation (8 categories) and the covariation model (Ronquist & Huelsenbeck 2003). Analyses were run as two separate chains (default heating parameters) for 20 million generations, by which time they had ceased converging (final average standard deviation of the split frequencies was less than 0.01). The quality of chains was estimated using built-in MrBayes tools. MrBayes program was run at the CIPRES ver. 3.3 website (Miller *et al.* 2010). Bayesian analysis quality was verified using the program Tracer ver. 1.7.1 (Rambaut *et al.* 2018).

Institutional acronyms

The specimens examined are kept at the following institutions and collections (the curator is given in parentheses):

SPbU = Department of Invertebrate Zoology, Faculty of Biology, St Petersburg University, Russia (Denis Tumanov)

ZM FEFU = Zoological Museum of Far Eastern Federal University, Vladivostok, Russia (Tatiana Savko)

Table 1 (continued on next page). Complete list of sequences used in the phylogenetic analysis. Sequences produced in this study are marked in bold.

	18S	28S	ITS-2	COI	References
Mesobiotus efa sp. nov.	**OR804457, OR804458, OR804459, OR804460**	**OR805135, OR805136, OR805137, OR805138, OR805139**	**OR805169, OR805170, OR805171**	**OR803035, OR803036, OR803037, OR803038, OR803039**	**This study**
Mesobiotus vulpinus sp. nov.	**OR804461, OR804462**	**OR805140, OR805141**	**OR805172, OR805173**	**OR803040, OR803041**	**This study**
Mesobiotus anastasiae	MT903468	MT903612	MT903470	MT904513	Tumanov 2020a
Mesobiotus cf. *barabanovi*	MN310392	MN310388	MN310390	MN313170	Kaczmarek *et al.* 2020
Mesobiotus datanlanicus	MK584659	MK584658	MK584657	MK578905	Stec 2019
Mesobiotus diegoi	OP142526, OP142527	OP142520, OP142521	OP142514, OP142515	OP143858, OP143857	Stec 2022
Mesobiotus dilimanensis	MN257048	MN257049	MN257050	MN257047	Itang *et al*. 2020
Mesobiotus ethiopicus	MF678793	MF678792	MN122776	MF678794	Stec & Kristensen 2017
Mesobiotus fiedleri	MH681585	MH681693	MH681724	MH676056	Kaczmarek *et al.* 2020
Mesobiotus harmsworthi	MH197146	MH197264	MH197154	MH195150, MH195151	Kaczmarek *et al*. 2018
Mesobiotus hilariae	KT226071			KT226108	Vecchi *et al*. 2016
Mesobiotus huecoensis	OQ756248			OQ756246	Vecchi *et al*. 2023
Mesobiotus imperialis	OL257855, OL257854	OL257867, OL257866		OL311514, OL311515	Stec 2021
Mesobiotus insanis	MF441488	MF441489	MF441490	MF441491	Mapalo *et al*. 2017
Mesobiotus maklowiczi	OP142525, OP142524	OP142518, OP142519		OP143855, OP143856	Stec 2022
Mesobiotus marmoreus	OL257856, OL257857, OL257858	OL257868, OL257869, OL257870	OL257861, OL257862, OL257863	OL311516, OL311517 OL311518	Stec 2021
Mesobiotus occultatus	MH197147, **OR794157**	**OR794158**	MH197155, **OR805249**	MH195152, **OR803042**	Kaczmarek *et al*. 2018; **This study**
Mesobiotus peterseni	OP142528, OP142529	OP142522, OP142523	OP142516, OP142517	OP143859, OP143860	Stec 2022
Mesobiotus philippinicus	KX129793	KX129794	KX129795	KX129796	Mapalo *et al.* 2016
Mesobiotus radiatus	MH197153	MH197152	MH197268, MH197267	MH195147, MH195148	Stec *et al*. 2018
Mesobiotus romani	MH197158	MH197151	MH197150	MH195149	Roszkowska *et al*. 2018
Mesobiotus harmsworthi gr.	MH197149	MH197266	MH197157	MH195154	

Table 1 (continued). Complete list of sequences used in the phylogenetic analysis. Sequences produced in this study are marked in bold.

	18S	28S	ITS-2	COI	References
Mesobiotus furciger gr.	MW751944, MW751946, MW751949, MW751952, MW751954, MW751955, MW751957, MW751959, MW751960, MW751962, MW751967, MW751934, MW751935, MW751936, MW751937, MW751939	MH197265	MH197156	MH195153, MW727932, MW727944, MW727933, MW727937, MW727938, MW727945, MW727941, MW727951 MW727953, MW727934, MW727939, MW727955, MW727956, MW727958, MW727961, MW727960	Kaczmarek *et al*. 2018; Short *et al.* 2022
Mesobiotus sp.	MW751942			MW727957	Short *et al.* 2022
Mesobiotus sp. Finland	OQ974689	OQ974704	OQ974696	OQ968323	Vecchi *et al*. 2024
Mesobiotus sp. Vietnam	OQ974691	OQ974705		OQ968314	Vecchi *et al*. 2024
Richtersius coronifer	MH681760	MH681757	MH681763	MH676053	Stec *et al*. 2020c

Results

Taxonomic account

Phylum Tardigrada Doyère, 1840
Class Eutardigrada Richters, 1926
Superfamily Macrobiotoidea Thulin, 1928
Family Macrobiotidae Thulin, 1928
Genus *Mesobiotus* Vecchi, Cesari, Bertolani, Jönsson, Rebecchi & Guidetti, 2016

Mesobiotus efa sp. nov.
urn:lsid:zoobank.org:act:EA291ABA-E1E5-4571-90AE-53D6A0DF530C
Figs 1–6; Tables 2–3

Etymology

Named after the children's teaching laboratory in St Petersburg "Efa". The studied material was collected during the field tip on the occasion of its anniversary.

Material examined

Holotype

RUSSIA • ♀; Leningrad Oblast, Vsevolozhsky District; a hill near the Lembolovo railway station, approx. 60.41612° N, 30.34266° E; 10 Sep. 2020; E. Androsova leg.; association of moss and lichen on soil; SPbU 275(72).

Paratypes

RUSSIA • 30 ♀♀, 14 eggs; same data as for holotype; SPbU 275(39, 47, 65–66, 68–72, 74–75, 77–80, 85–88, 104–106, 133–134, 136, 143, 147, 155, 182, 197, 207–208, 210–213) • 1 adult, 2 eggs; same data as for holotype; SEM stub SPbU Tar_33 • 2 adults; same data as for holotype; ZM FEFU (slides 275(73), 275(76)) • 2 eggs; same data as for holotype; ZM FEFU (slides 275(67) and 275(180)).

Morphological description

Adult animals

Body elongated (Fig. 1) (morphometrics in Table 2, raw morphometric data are provided in the Supp. file 4). Fresh specimens uncolored or whitish with slightly greenish gut content, transparent after fixation in Hoyer's medium. Black eyes present (Figs 1A, 3A, black arrowheads), often dissolving after slide mounting. Cuticle smooth in LM, with fine uniform sculpture consisting of minute conical granules with pointed apices visible under SEM only (Fig. 2A). All legs with granulated areas consisted of small granules, poorly discernible or, sometimes, completely invisible in LM. Legs I–III with small granulated areas on the external surfaces, near the claw bases (Fig. 2B–C), the internal leg surfaces without granulation, with distinct pulvinus. Legs IV with better-developed granulation mainly dorsally to the claws (Fig. 2D) and around the claw bases (Fig. 4C–D, white arrowhead).

Buccal-pharyngeal apparatus of *Macrobiotus* type (Fig. 3A) with the ventral lamina and ten peribuccal lamellae. Oral cavity armature (OCA) of *harmsworthi* type (according to Kaczmarek *et al*. 2020) with three bands of teeth visible in LM. Evident first (anterior) band consists of a wide band of numerous

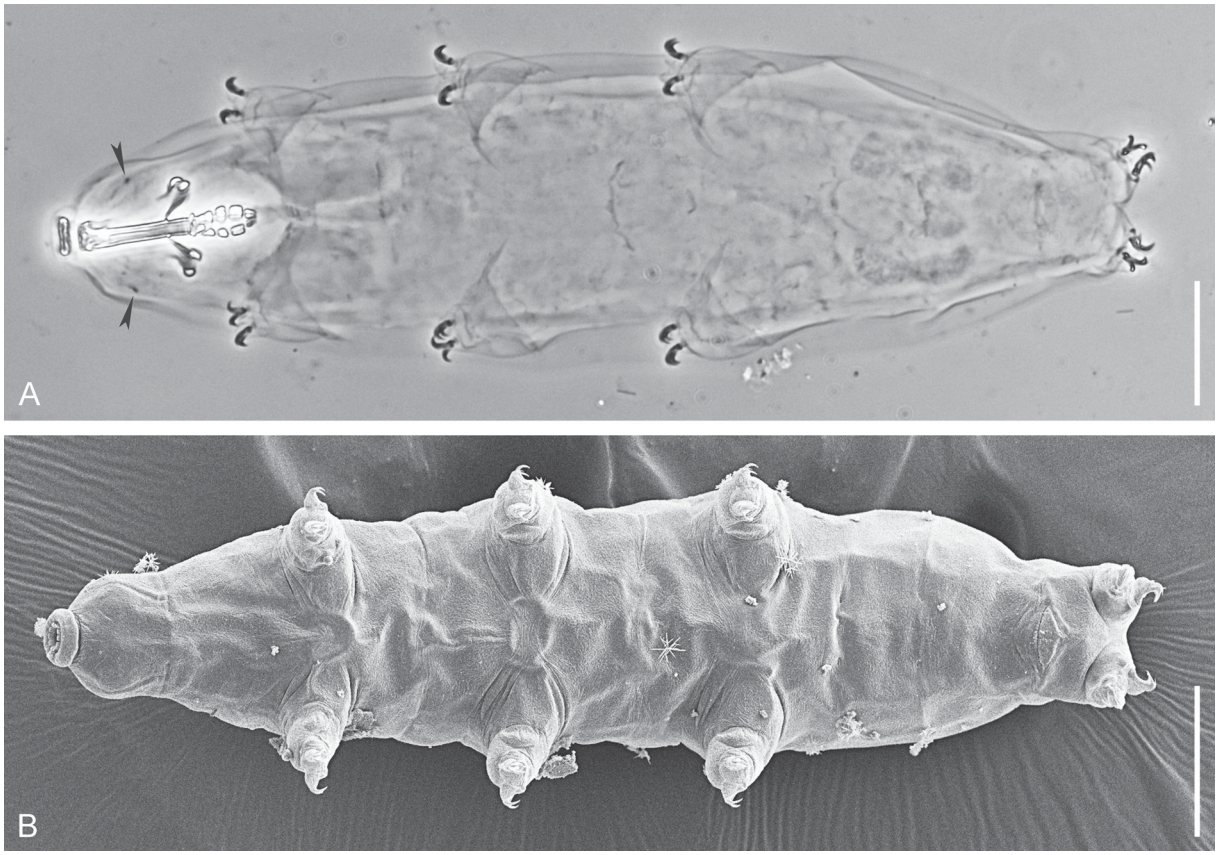

Fig. 1. *Mesobiotus efa* sp. nov., total view. **A**. Holotype, ♀ (SPbU 275(72)). Dorso-ventral view, black arrowheads indicate eyes, PhC. **B**. Paratype (SPbU Tar_33). Ventral view in SEM. Scale bars = 50 µm.

minute teeth visible as dots in LM (Fig. 3D, F–G). Second band consists of a row of longitudinally elongated triangular teeth (Fig. 3D–G). Third band comprises three dorsal and three ventral transverse ridges (Fig. 3D–G). Medio-ventral ridge usually never divided into separate parts, only single specimen was found with detached lateral part of the medio-ventral ridge. Ventrally OCA with numerous additional teeth between the second and the third teeth bands (Fig. 3F–G). Pharyngeal bulb with apophyses, three macroplacoids and a large microplacoid (Fig. 3B–C). Macroplacoid length sequence is $2 < 3 \leq 1$. First macroplacoid is anteriorly narrowed, third macroplacoid with distinct subterminal constriction (Fig. 3B–C).

Claws of *Mesobiotus* type with minute stalk, distinct distal part of the basal portion, short common tract and developed internal septum, defining a distal part (Fig. 4A–C, E). Primary and secondary branches diverge below the half of the claw height, main branches with well-developed accessory points (Fig. 4A,

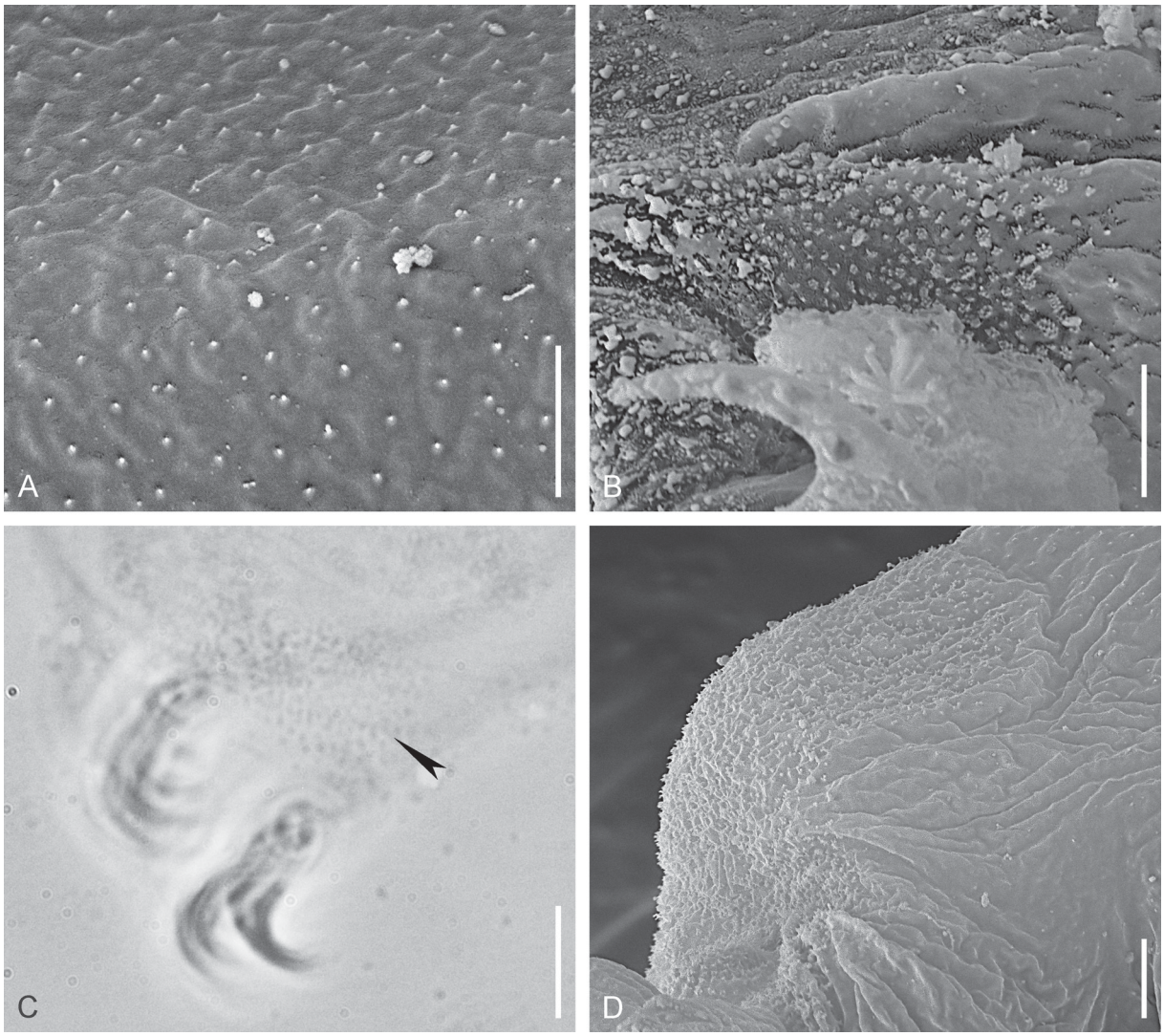

Fig. 2. *Mesobiotus efa* sp. nov., cuticular sculpture. **A–B, D**. Paratype (SPbU Tar_33). **C**. Paratype (SPbU 275(197)). **A**. High magnification of the sculpture of the dorsal body surface, SEM. **B**. Dot-like sculpture on the external surface of leg III, SEM. **C**. Dot-like sculpture on the external surface of leg III, PhC, black arrowhead indicates dots. **D**. Dot-like sculpture on the dorsal side of hind legs, SEM. Scale bars: A–B, D = 2 μm; C = 5 μm.

C–D). Claws of fourth pair of legs slightly longer than claws of first three pairs of legs (Fig. 4C). All claws with smooth lunules (Fig. 4). Anterior (internal) and posterior (external) claws of the legs IV are similar in shape (Fig. 4D). Lunules on posterior claws distinctly larger than on anterior claws (Fig. 4C–D). Single continuous cuticular bars are present below claw bases of the first three pairs of legs (Fig. 4A–B, black arrowhead) with poorly developed muscle attachment points below (Fig. 4B). Claws of the legs IV are connected with a wide but poorly sclerified horseshoe-like structure, visible in PhC only (Fig. 4E, black arrowhead).

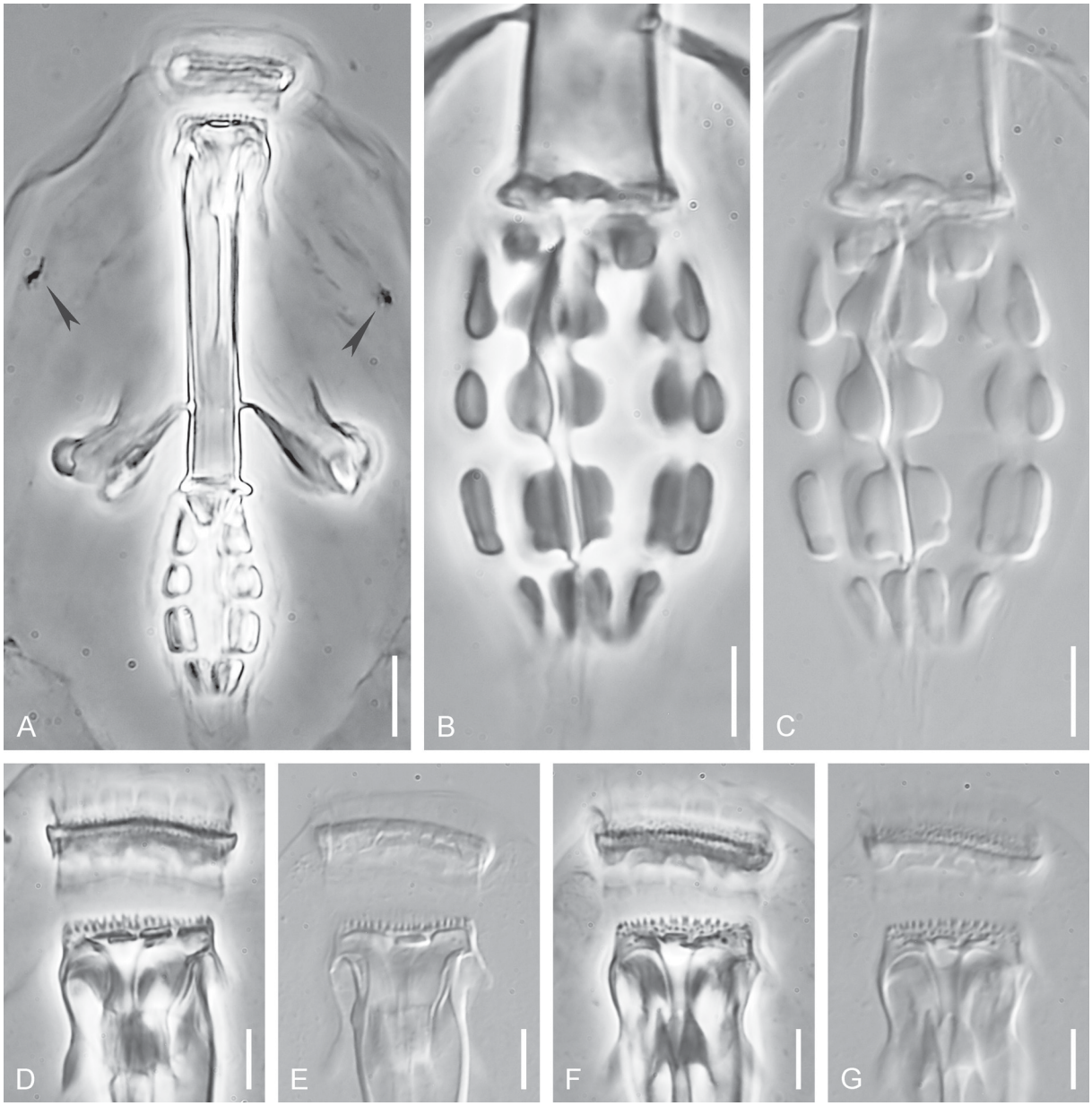

Fig. 3. *Mesobiotus efa* sp. nov., bucco-pharyngeal apparatus. **A**. Holotype (SPbU 275(72)). **B–G**. Paratype (SPbU 275(197)). **A**. Total dorso-ventral view of the bucco-pharyngeal apparatus, black arrowheads indicate eyes, PhC. **B–C**. Placoids, PhC (B) and DIC (C). **D–G**. Oral cavity armature (D–E = dorsal view, F–G = ventral view), PhC (D, F), DIC (E, G). Scale bars: A = 10 µm; B–G = 5 µm.

Table 2. Summary of morphometric data for *Mesobiotus efa* sp. nov. Measurements are given in µm, *pt* values in % (the *pt* index is the percentage ratio between the length of a structure and the length of the buccal tube).

CHARACTER	N	RANGE						MEAN		SD		Holotype	
		µm			*pt*			µm	*pt*	µm	*pt*	µm	*pt*
Body length	17	238	–	430	*759*	–	*1048*	321	*856*	51	*72*	430	*940*
Buccopharyngeal tube													
Buccal tube length	21	29.7	–	45.8		–		38.1	–	4.5	–	45.8	–
Stylet support insertion point	21	22.6	–	35.3	*74.0*	–	*78.8*	29.3	*77.0*	3.5	*1.0*	35.3	*77.2*
Buccal tube external width	21	4.1	–	8.6	*12.1*	–	*19.6*	5.6	*14.6*	1.0	*1.5*	6.7	*14.7*
Buccal tube internal width	21	3.1	–	7.6	*8.4*	–	*17.2*	4.2	*10.9*	1.0	*1.6*	5.0	*10.9*
Ventral lamina length	19	17.3	–	27.2	*56.6*	–	*61.4*	22.4	*59.5*	2.9	*1.4*	27.2	*59.5*
Placoid lengths													
Macroplacoid 1	21	2.3	–	6.5	*7.7*	–	*15.6*	4.7	*12.1*	1.1	*1.9*	5.9	*12.9*
Macroplacoid 2	21	2.4	–	5.1	*7.9*	–	*12.6*	3.8	*9.9*	0.7	*1.1*	4.7	*10.3*
Macroplacoid 3	21	2.7	–	6.5	*9.2*	–	*14.2*	4.6	*11.9*	1.0	*1.4*	6.5	*14.1*
Microplacoid	21	1.6	–	4.9	*5.5*	–	*11.2*	3.6	*9.4*	0.8	*1.6*	4.8	*10.5*
Macroplacoid row	21	9.3	–	18.6	*31.3*	–	*45.3*	14.6	*38.2*	2.5	*3.4*	18.3	*40.0*
Placoid row	21	12.5	–	24.0	*42.0*	–	*56.9*	18.9	*49.4*	3.1	*3.6*	24.0	*52.5*
Claw 1 lengths													
External primary branch	18	6.0	–	9.4	*17.6*	–	*22.5*	7.5	*20.0*	1.0	*1.2*	?	*?*
External secondary branch	18	5.0	–	8.0	*13.3*	–	*18.1*	6.1	*16.3*	0.8	*1.1*	?	*?*
Internal primary branch	21	5.7	–	9.1	*17.1*	–	*21.0*	7.3	*19.1*	0.9	*0.9*	9.1	*19.9*
Internal secondary branch	21	4.3	–	8.1	*13.9*	–	*17.6*	6.0	*15.7*	0.9	*1.0*	8.1	*17.6*
Claw 2 lengths													
External primary branch	20	6.2	–	9.7	*19.1*	–	*22.8*	7.9	*20.7*	1.0	*1.1*	9.7	*21.1*
External secondary branch	20	5.3	–	8.9	*15.1*	–	*19.4*	6.5	*17.0*	0.9	*1.2*	8.9	*19.4*
Internal primary branch	20	5.7	–	9.1	*18.0*	–	*21.8*	7.2	*19.0*	0.9	*0.9*	9.1	*19.8*
Internal secondary branch	20	4.5	–	7.8	*14.4*	–	*18.1*	6.1	*16.0*	0.8	*1.2*	6.7	*14.6*
Claw 3 lengths													
External primary branch	20	6.4	–	9.7	*19.3*	–	*23.0*	7.9	*20.8*	1.0	*1.0*	9.7	*21.1*
External secondary branch	20	5.3	–	8.4	*14.9*	–	*19.0*	6.3	*16.7*	0.8	*1.1*	7.8	*17.0*
Internal primary branch	20	5.8	–	9.1	*17.1*	–	*21.3*	7.3	*19.2*	0.9	*1.0*	9.1	*19.8*
Internal secondary branch	20	4.7	–	7.9	*14.1*	–	*17.8*	6.1	*16.1*	0.7	*0.9*	6.9	*15.2*
Claw 4 lengths													
Anterior primary branch	19	6.6	–	10.8	*16.8*	–	*27.5*	8.8	*23.3*	1.2	*2.4*	9.9	*21.6*
Anterior secondary branch	19	5.1	–	8.4	*16.3*	–	*19.9*	7.0	*18.4*	0.9	*1.1*	7.5	*16.3*
Posterior primary branch	16	7.6	–	11.6	*22.4*	–	*29.0*	9.5	*25.4*	1.2	*1.4*	?	*?*
Posterior secondary branch	15	5.4	–	8.0	*16.4*	–	*20.1*	6.8	*18.2*	0.8	*1.0*	?	*?*

Eggs

One adult female with mature oocites was islolated and cultivated for three days until the eggs were layed. After that the female was taken for the DNA extraction and gene sequencing (voucher slide SPbU 275(211)) while the layed eggs were taken for the morphological analysis using LM.

Eggs spherical, white, ornamented and laid freely (Figs 5A–C, 6A; morphometrics in Table 3). Chorion with conical processes that can be attributed to the "cones with long slender endings and filaments" and "reticular design with "bubbles" morphotypes" (according to Kaczmarek *et al*. 2020). Egg processes with wide bases and thinned and flexible apices usually well differentiated (Figs 5, 6A–B, D). Processes (with the exception of the thinned apical parts) with bilayered walls, with a net of trabecular structures between the internal and external layers, forming irregular rounded meshes of different size, so the processes seem to be reticulated in LM (Fig. 5). Apical parts of the processes with bubble-like internal

Table 3. Measurements (in µm) of selected morphological structures of eggs of *Mesobiotus efa* sp. nov. Abbreviations: N = number of eggs/structures measured, range refers to the smallest and the largest structure among all measured specimens; SD = standard deviation).

CHARACTER	N	RANGE	MEAN	SD
Egg bare diameter	10	67.5 – 69.1	68.3	1.1
Egg full diameter	10	97.3 – 104.1	100.7	4.8
Process height	30	11.1 – 21.6	15.0	2.4
Process base width	30	7.6 – 14.2	10.3	1.6
Process base/height ratio	30	49% – 103%	70%	12%
Inter-process distance	15	2.2 – 6.6	4.4	1.3
Number of processes on the egg circumference	10	12 – 14	13.0	1.4

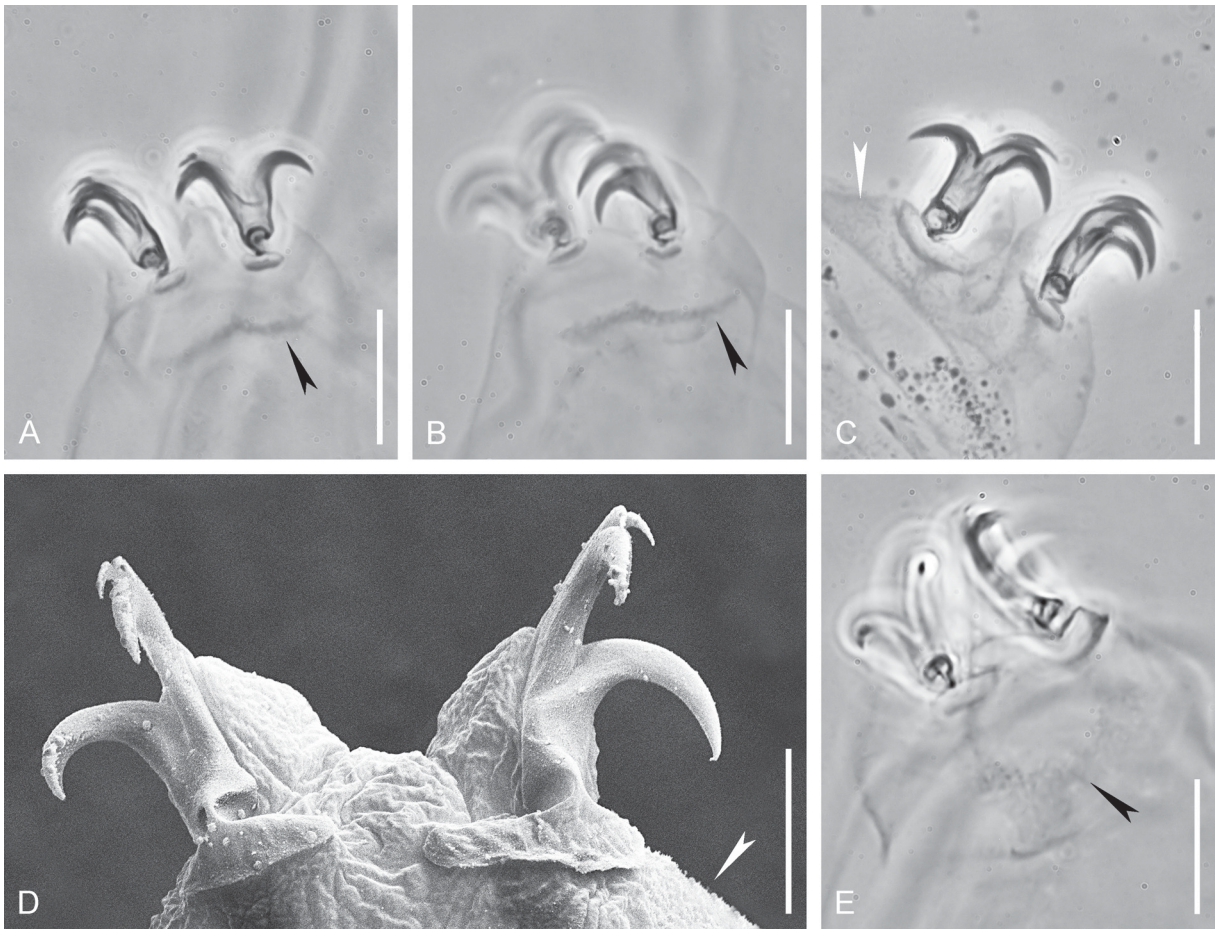

Fig. 4. *Mesobiotus efa* sp. nov., claws. **A–B, E**. Holotype (SPbU 275(72)). **C**. Paratype (SPbU 275(197)). **D**. Paratype (SPbU Tar_33). **A**. Claws of leg I, black arrowhead indicates bar-like cuticular thickening, PhC. **B**. Claws of leg II, black arrowhead indicates bar-like cuticular thickening, PhC. **C**. Claws of leg IV, white arrowhead indicates cuticular sculpture around the claw base, PhC. **D**. Claws of leg IV, white arrowhead indicates cuticular sculpture around the claw base, SEM. **E**. Claws of leg IV, black arrowhead indicates horseshoe-like structure, PhC. Scale bars: A–C, E = 10 µm; D = 5 µm.

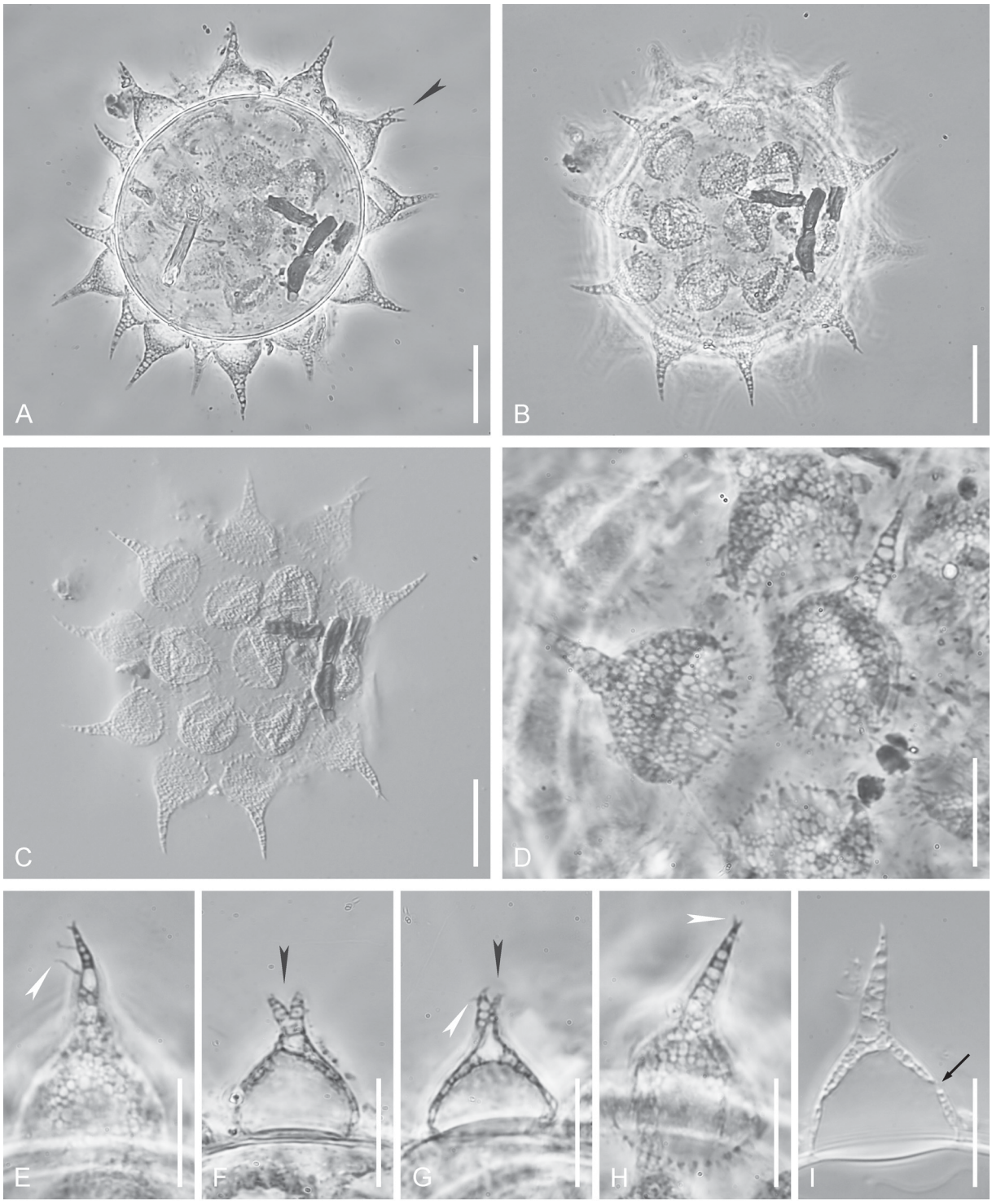

Fig. 5. *Mesobiotus efa* sp. nov., eggs. **A–E, H–I**. Paratype (SPbU 275(210)). **F–G**. Paratype (SPbU 275(180)). **A**. Total view of the optical section of the embryonated egg, PhC. **B**. Total view of the egg surface, PhC. **C**. Total view of the egg surface, DIC. **D**. Details of the egg surface, PhC. **E–H**. Egg processes, PhC. **I**. Optical section of the egg process, DIC. Black arrowheads indicate bifurcated tips, white arrowheads indicate terminal and subterminal filaments, black arrow indicates a pore. Scale bars: A–C = 20 μm; D–I = 10 μm.

structure (Fig. 5), rarely bifurcating (Fig. 5A, F–G, black arrowheads), usually with a tuft of very short (0.5–2,75 μm) apical and subapical filaments (Figs 5E, G–H, 6D, white arrowheads). Large pores (ca 1 μm in diameter), mostly indiscernible in LM and well-visible in SEM, are present on the basal part of all processes, forming a single row (Figs 5I, black arrowhead, 6B–D, black arrowheads). Process bases with well-developed crone of dark thickenings, visible in LM (Fig. 5A–D, H). Egg surface between the processes without areolation or pores but with a system of irregularly distributed wrinkles poorly discernible in LM as irregularly distributed granules and well-visible in SEM (Figs 5D, 6A–C).

Reproduction

No males were found.

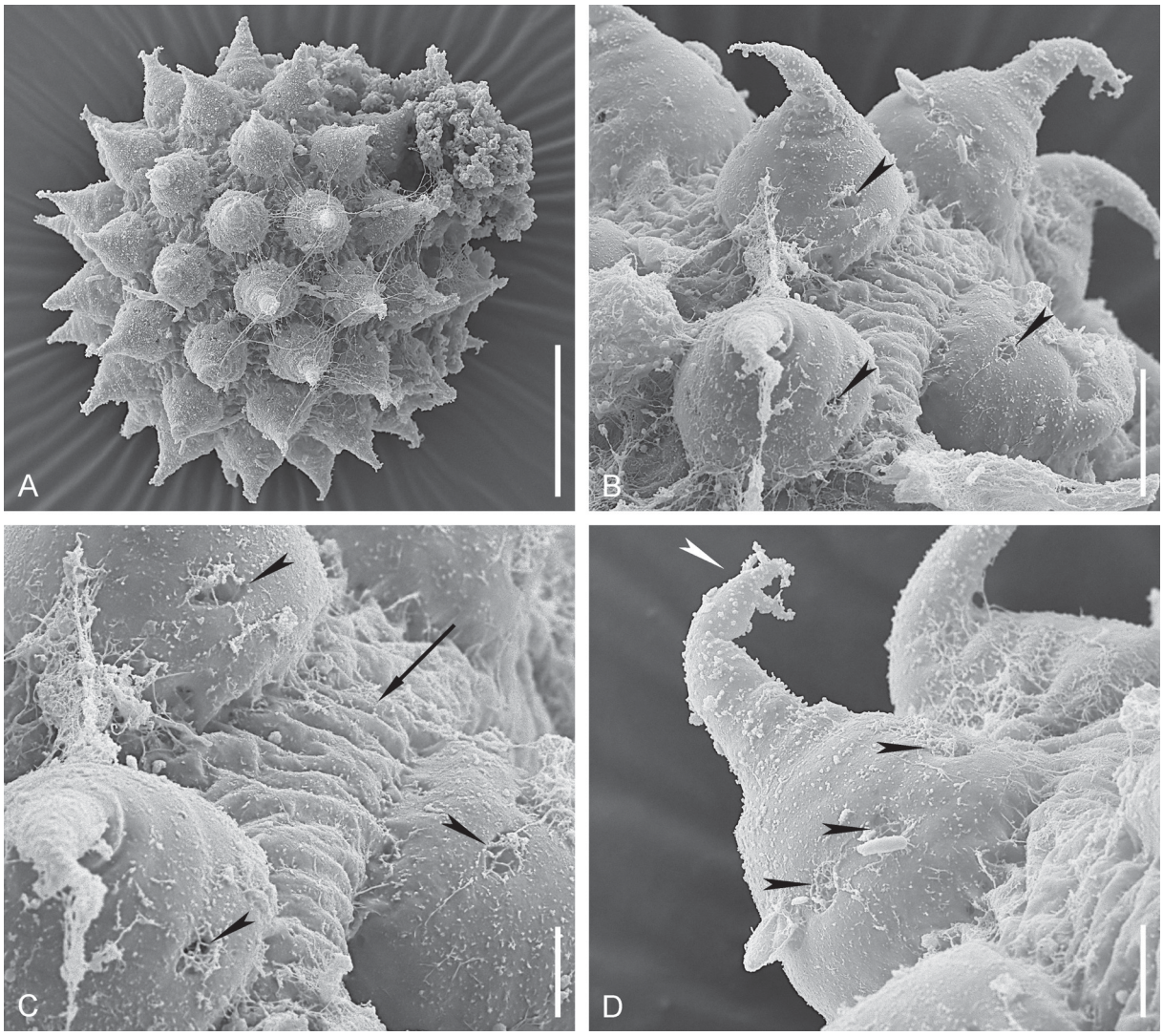

Fig. 6. *Mesobiotus efa* sp. nov., paratype (SPbU Tar_33), eggs. **A**. Total view of the egg, SEM. **B–C**. Details of the egg surface, black arrowheads indicate pores on the egg processes, black arrow indicates wrinkles on the egg surface, SEM. **D**. Egg process, black arrowheads indicate pores, white arrowhead indicates terminal filaments, SEM. Scale bars: A = 20 μm; B = 5 μm; C–D = 2 μm.

DNA sequences

Sequences for 18S rRNA marker were obtained from four specimens (accession numbers: OR804457–OR804460; voucher slides: SpbU 275(077, 104–106)). Sequences for 28S rRNA and COI markers were obtained from five specimens (accession numbers: OR805135–OR805139 and OR803035–OR803039 respectively; voucher slides SpbU 275(077, 104–106, 211). Sequences for ITS-2 marker were obtained from three specimens (accession numbers: OR805169–OR805171; voucher slides SpbU 275(077, 104, 211). Presence of two COI haplotypes was revealed.

Mesobiotus vulpinus sp. nov.
urn:lsid:zoobank.org:act:CC615859-F0A0-49F4-A035-28889F370283
Figs 7–13; Tables 4–5

Etymology

Named after the latin name (*Vulpes vulpes*) of the most famous animal inhabiting Russkij Island – the common fox.

Material examined

Holotype

RUSSIA • ♀; Primorsky Krai, Vladivostok, Russkij Island, road to the Kruglaja Bay; 43.01386° N, 131.78838° E; 3 Feb. 2023; A. Kalimullin leg.; moss on tree trunk; SPbU 320(10).

Paratypes

RUSSIA • 8 ♀♀, 4 eggs; same data as for holotype; SPbU 320(2–9, 11, 13–15) • 2 adult, 2 eggs; same data as for holotype; SEM stub SPbU Tar_65 • 1 adult; same data as for holotype; ZM FEFU (slide 320(1)) • 1 egg; same data as for holotype; ZM FEFU (slide 320(12)).

Morphological description

Adult animals

Body elongated (Fig. 7) (morphometrics in Table 4, raw morphometric data are provided in the Supp. file 5). Fresh specimens uncolored or whitish with slightly greenish gut content, transparent after fixation in Hoyer's medium. Black eyes present, often dissolving after slide mounting. Cuticle smooth in LM, with fine uniform sculpture consisting of minute conical granules with pointed apices visible under SEM only (Fig. 8A). All legs with granulated areas consisted of small granules, usually well visible in LM. Legs I–III with small granulated areas on the external surfaces, near the claw bases (Fig. 8B–C, black arrowhead), the internal leg surfaces without granulation, with indistinctly demarcated large pulvinus, visible in SEM only (Fig. 10A, white arrowhead). Legs IV with better-developed granulation mainly dorsally to the claws (Fig. 8D–E, white arrowhead) and around the claw bases (Fig. 10E, H, black arrowheads).

Buccal-pharyngeal apparatus of *Macrobiotus* type (Fig. 9A) with the ventral lamina and ten peribuccal lamellae (Fig. 8F). Oral cavity armature (OCA) of *harmsworthi* type (according to Kaczmarek *et al*. 2020) with three bands of teeth visible in LM. Evident first (anterior) band consists of a wide band of numerous minute teeth visible as dots in LM (Figs 8F, white arrow, 9E, G). Second band consists of a row of longitudinally elongated triangular teeth (Fig. 9D–H). Third band comprises three dorsal and three ventral transverse ridges (Figs 8F white arrowhead, 9D–H). Medio-ventral ridge often divided in two or three separate teeth (Fig. 9H). Latero-ventral ridges often with strong indentations (Fig. 9G), sometimes almost fragmented to separate teeth. Rare additional teeth are present ventrally, between the second and the third teeth bands (Fig. 9F–H). Pharyngeal bulb with apophyses, three macroplacoids and a large microplacoid (Fig. 9B–C). Macroplacoid length sequence is $2 < 3 \leq 1$. First macroplacoid is anteriorly narrowed, third macroplacoid with poorly developed subterminal constriction (Fig. 9B–C).

Claws of *Mesobiotus* type with minute stalk, distinct distal part of the basal portion, short common tract and developed internal septum, defining a distal part (Fig. 10B, D–E). Primary and secondary branches diverge below the half of the claw height, main branches with well-developed accessory points (Fig. 10B–F). Claws of fourth pair of legs slightly longer than claws of first three pairs of legs (Fig. 10E). All claws with smooth lunules (Fig. 10B–C, E, G). Anterior (internal) and posterior (external) claws of the legs IV are similar in shape (Fig. 10E). Single continuous cuticular bars of characteristic shape (two wide short bars connected by thin angular strip) are present below claw bases of the first three pairs of legs (Fig. 10B, D, black arrowhead) with poorly developed muscle attachment points below (Fig. 10B, D). Claws of the legs IV are connected with a poorly sclerified horseshoe-like structure, visible in PhC only (Fig. 10H, white arrowhead).

Eggs

No eggs with developed embryos were found, but taking into account that *M. vulpinus* sp. nov. was the only tardigrade species present in the sample we believe that the adult specimens and the eggs belong to the same species.

Eggs spherical, white, ornamented and laid freely (Figs 11A, 12A, C; morphometrics in Table 5). Chorion with conical processes that can be attributed to the "sharp narrow cones" and "reticular design with "bubbles" morphotypes" (according to Kaczmarek *et al*. 2020). Egg processes in form of elongated cones with poorly differentiated basal and apical parts (Figs 11B, E–F, 12–13). Processes (with the

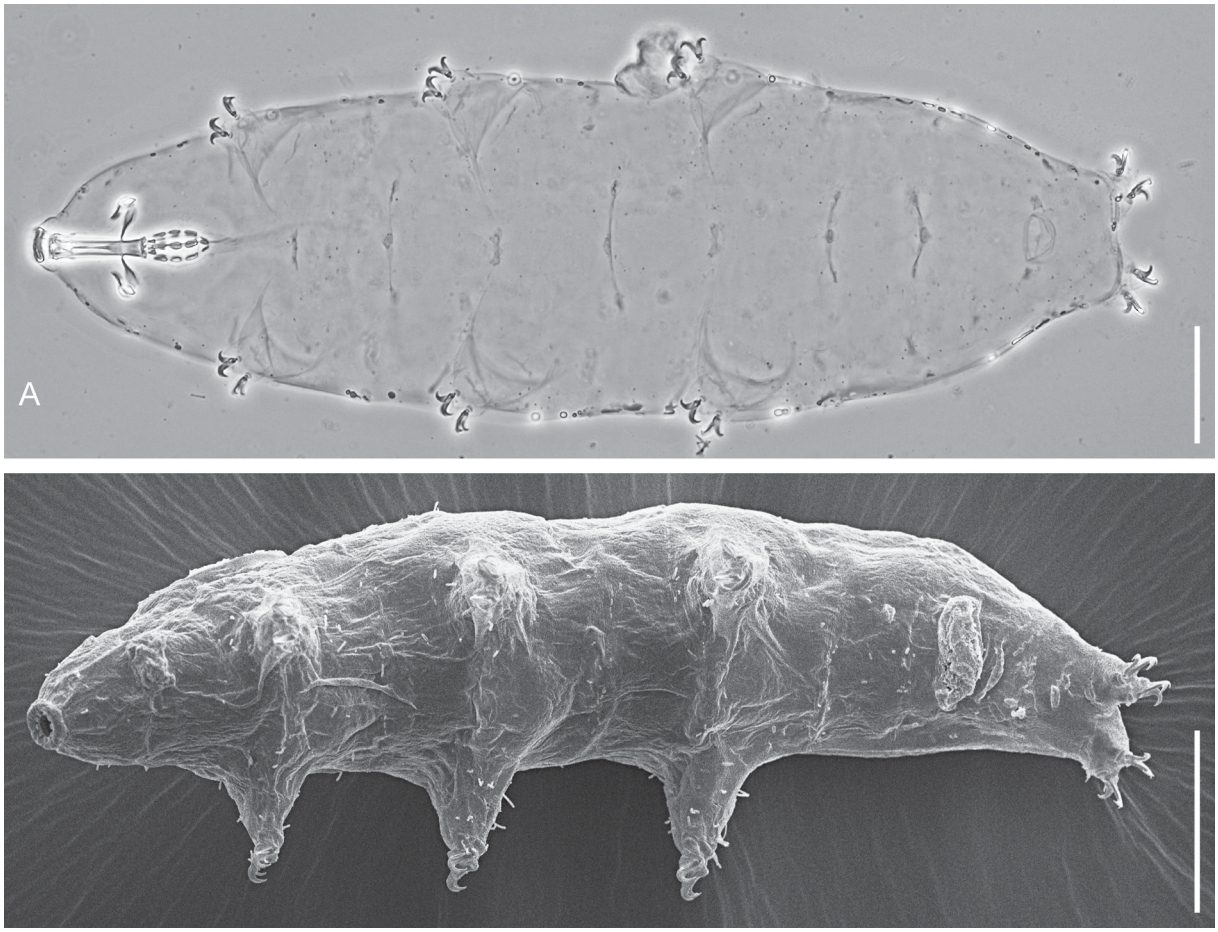

Fig. 7. *Mesobiotus vulpinus* sp. nov., total view. **A**. Paratype, ♀ (SPbU 420(1)). Dorso-ventral view, PhC. **B**. Paratype (SPbU Tar_65). Ventro-lateral view in SEM. Scale bars = 50 µm.

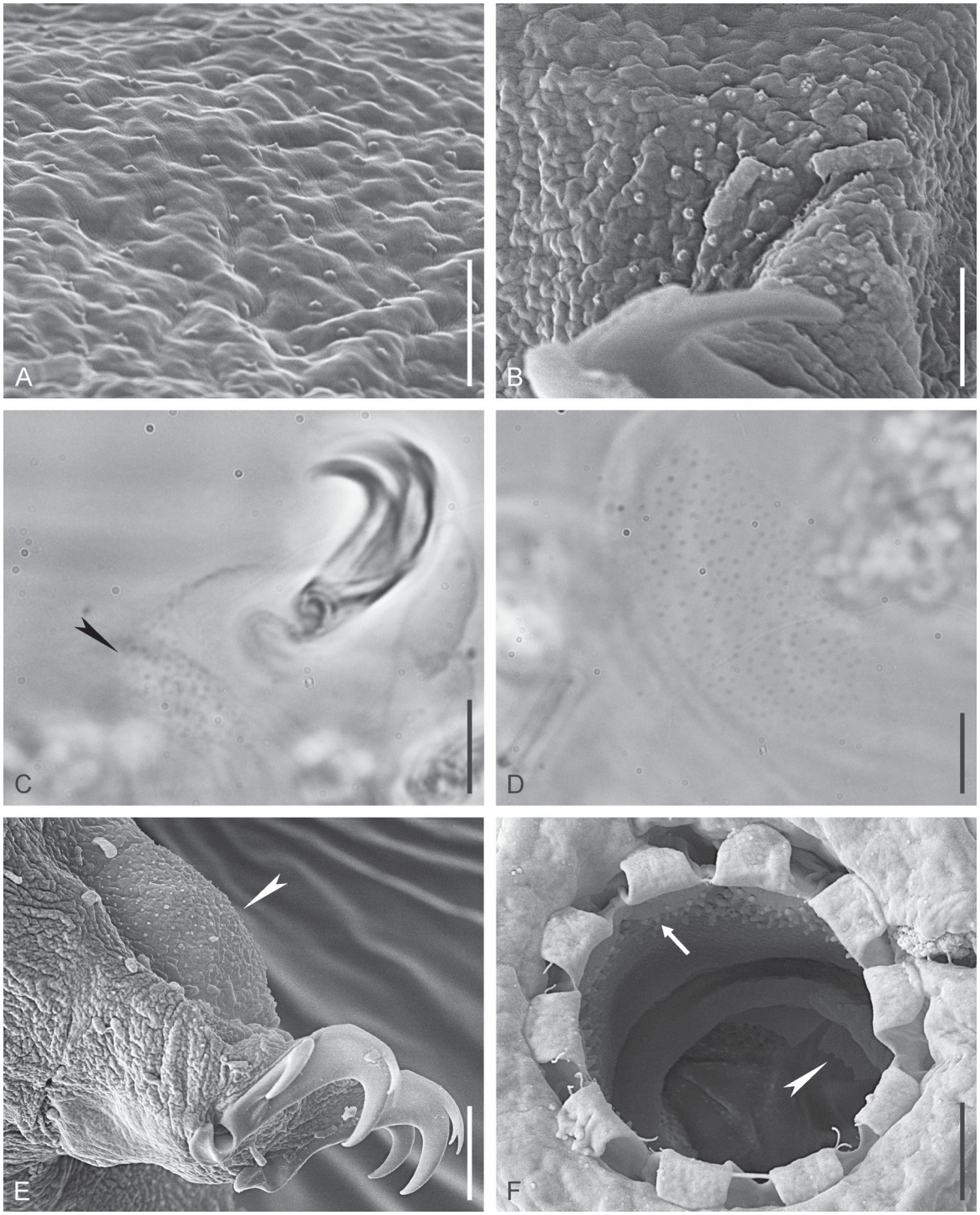

Fig. 8. *Mesobiotus vulpinus* sp. nov., cuticular sculpture and oral cavity armature (OCA). **A–B, E–F**. Paratype (SPbU Tar_33). **C–D**. Holotype (SPbU 320(10)). **A**. High magnification of the sculpture of the dorsal body surface, SEM. **B**. Dot-like sculpture on the external surface of leg III, SEM. **C**. Dot-like sculpture on the external surface of leg III, PhC, black arrowhead inticates the zone of sculpture. **D**. Dot-like sculpture on the dorsal side of hind leg, PhC. **E**. Dot-like sculpture on the dorsal side of hind leg, SEM, white arrowhead indicates the zone of sculpture. **F**. Mouth opening with dorsal OCA visible, SEM, white arrow indicates the first band of teeth, white arrowhead indicates the dorsal crests of the third band of teeth. Scale bars A–B, F = 2 μm; C–E = 5 μm.

Table 4. Summary of morphometric data for *Mesobiotus vulpinus* sp. nov. Measurements are given in µm, *pt* values in % (the *pt* index is the percentage ratio between the length of a structure and the length of the buccal tube).

CHARACTER	N	RANGE						MEAN		SD		Holotype	
		µm			*pt*			µm	*pt*	µm	*pt*	µm	*pt*
Body length	10	264	–	521	*808*	–	*1119*	366	*948*	87	*121*	521	*1119*
Buccopharyngeal tube													
Buccal tube length	10	30,1	–	46,5		–		38,3	–	5,7	–	46,5	–
Stylet support insertion point	10	22,5	–	35,2	*74,7*	–	*77,6*	29,0	*75,8*	4,5	*0,8*	35,2	*75,6*
Buccal tube external width	10	4,0	–	7,6	*13,0*	–	*18,2*	5,6	*14,6*	1,2	*1,4*	7,2	*15,5*
Buccal tube internal width	10	2,9	–	6,0	*9,6*	–	*14,4*	4,3	*11,1*	1,1	*1,5*	5,6	*12,0*
Ventral lamina length	9	20,0	–	32,1	*61,7*	–	*69,0*	25,4	*66,1*	4,4	*2,3*	32,1	*69,0*
Placoid lengths													
Macroplacoid 1	10	3,4	–	6,4	*10,9*	–	*15,3*	5,0	*12,9*	1,1	*1,6*	6,4	*13,7*
Macroplacoid 2	10	3,0	–	5,7	*9,7*	–	*12,4*	4,1	*10,6*	0,9	*0,8*	5,4	*11,5*
Macroplacoid 3	10	3,0	–	6,4	*9,9*	–	*14,3*	4,9	*12,6*	1,1	*1,3*	6,4	*13,7*
Microplacoid	10	2,0	–	4,5	*6,5*	–	*9,9*	3,3	*8,5*	0,8	*1,0*	4,5	*9,7*
Macroplacoid row	10	11,2	–	21,3	*37,4*	–	*46,6*	16,2	*41,9*	3,4	*3,1*	21,3	*45,7*
Placoid row	10	14,3	–	27,3	*47,4*	–	*58,9*	20,5	*53,2*	4,2	*3,7*	27,3	*58,6*
Claw 1 heights													
External primary branch	10	7,2	–	12,4	*22,0*	–	*26,7*	9,4	*24,7*	1,5	*1,3*	12,4	*26,7*
External secondary branch	10	5,7	–	9,6	*18,5*	–	*23,2*	7,6	*19,9*	1,2	*1,4*	9,6	*20,5*
Internal primary branch	10	6,8	–	12,6	*22,7*	–	*27,0*	9,3	*24,2*	1,6	*1,3*	12,6	*27,0*
Internal secondary branch	10	5,5	–	9,2	*16,2*	–	*22,3*	7,3	*19,1*	1,2	*1,6*	8,9	*19,2*
Claw 2 heights													
External primary branch	10	7,5	–	13,3	*23,0*	–	*28,5*	9,8	*25,6*	1,7	*1,6*	13,3	*28,5*
External secondary branch	10	5,9	–	11,1	*19,0*	–	*23,8*	8,2	*21,3*	1,5	*1,7*	11,1	*23,8*
Internal primary branch	10	8,1	–	12,5	*24,2*	–	*28,0*	10,0	*26,1*	1,4	*1,1*	12,5	*26,8*
Internal secondary branch	10	5,5	–	9,0	*17,9*	–	*24,4*	7,8	*20,4*	1,1	*1,9*	9,0	*19,4*
Claw 3 heights												?	*?*
External primary branch	10	7,8	–	13,0	*23,7*	–	*27,8*	9,9	*25,8*	1,5	*1,3*	13,0	*27,8*
External secondary branch	10	5,6	–	9,8	*17,2*	–	*22,4*	7,7	*20,1*	1,4	*1,6*	9,8	*21,0*
Internal primary branch	10	7,8	–	12,6	*24,2*	–	*28,9*	9,9	*25,9*	1,5	*1,4*	12,6	*27,0*
Internal secondary branch	10	6,1	–	10,4	*17,9*	–	*26,9*	7,9	*20,7*	1,4	*2,4*	9,1	*19,5*
Claw 4 heights													
Anterior primary branch	10	8,7	–	14,6	*27,5*	–	*32,2*	11,4	*29,8*	1,8	*1,4*	14,6	*31,4*
Anterior secondary branch	10	5,9	–	10,8	*19,7*	–	*23,4*	8,4	*22,0*	1,4	*1,3*	10,8	*23,2*
Posterior primary branch	10	9,5	–	13,5	*27,1*	–	*35,1*	11,8	*31,1*	1,6	*2,4*	12,6	*27,1*
Posterior secondary branch	10	7,4	–	11,0	*20,1*	–	*25,3*	8,9	*23,5*	1,3	*1,7*	9,8	*21,0*

exception of the elongated apical parts) with bilayered walls, with a net of trabecular structures between the internal and external layers, forming irregular rounded meshes of different size, so the processes seem to be reticulated in LM (Fig. 11). Apical parts of the processes with bubble-like internal structure (Fig. 11F), rarely bifurcating (Figs 11E, 13A). Processes surface bears annulations, visible in SEM only (Figs 12B, D, 13). Rare large pores (1.4–2.3 µm in diameter), poorly discernible in LM and well-visible in SEM, are present on the basal part of all processes, below the half of the process height, forming a single row (Figs 11H, white arrowheads, 12, 13, white arrowheads), Second row of distinctly smaller and more numerous pores is located in the most basal part of each process (Fig. 13, black arrowheads). Process bases with poorly developed, sometimes almost invisible crone of dark thickenings (Fig. 11C, E–F). Egg surface between the processes with distinct polygonal relief consisted of ridges forming hexagonal (rarely pentagonal) cells around each process (Figs 11C–D, 12). Points of ridges intersection bears small bulbous processes (Figs 11B, 12B, D, 13B). Both ridges and bulbous processes with internal trabecular structures, similar to the main processes walls. Egg surface between the processes bases and

the ridges of polygonal relief with a system of smaller radial ridges and pores discernible both in LM and SEM (Figs 11C–D, 12B, D, 13).

Reproduction

No males were found.

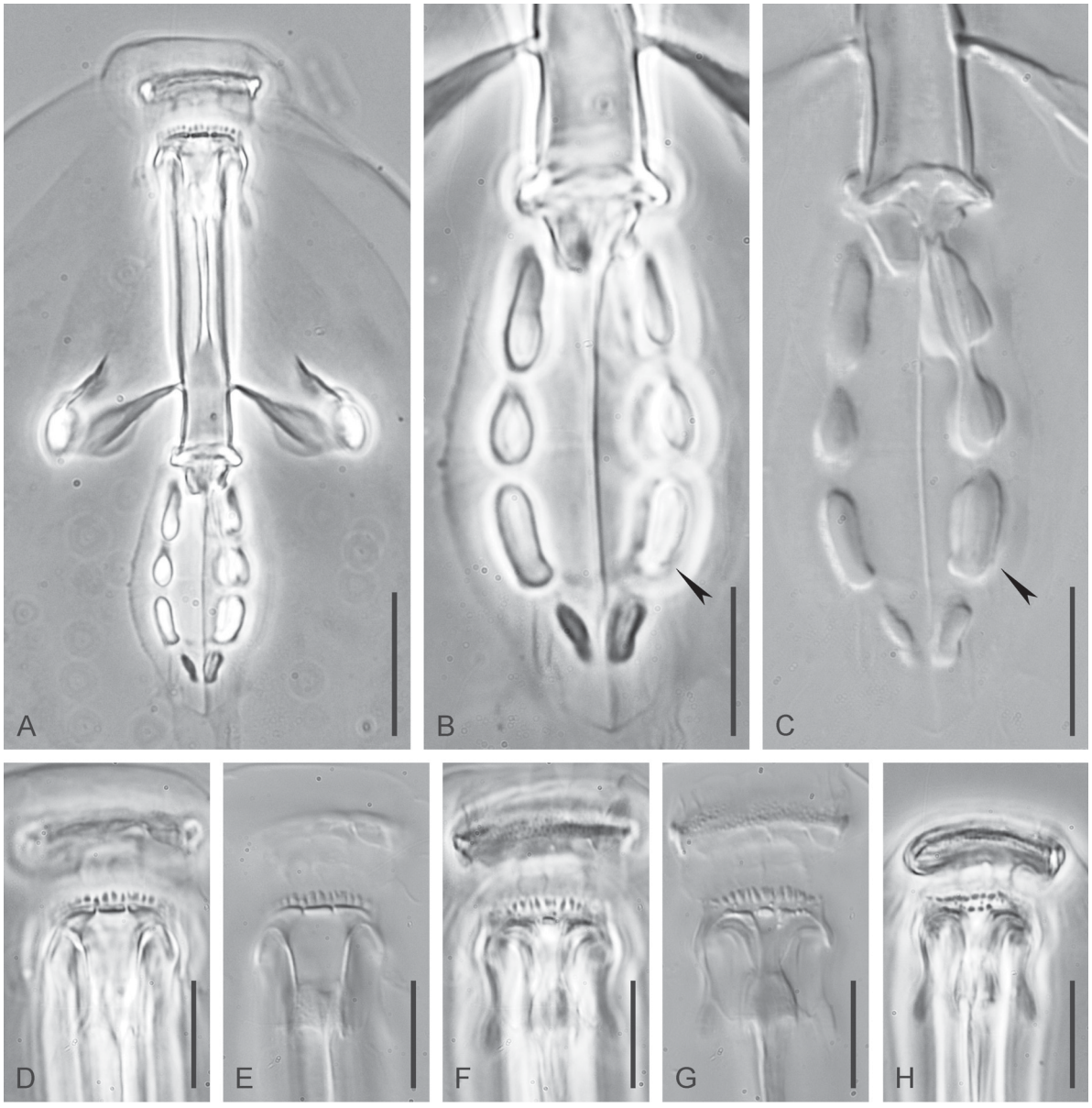

Fig. 9. *Mesobiotus vulpinus* sp. nov., bucco-pharyngeal apparatus. **A–G**. Holotype (SPbU 320(10)). **H**. Paratype (SPbU 320(1)). **A**. Total dorso-ventral view of the bucco-pharyngeal apparatus, PhC. **B–C**. Placoids, black arrowheads indicate the preterminal constriction of the third macroplacoid, PhC (B), DIC (C). **D–G**. Oral cavity armature (D–E = dorsal view, F–G = ventral view), PhC (D, F), DIC (E, G). **H**. Oral cavity armature with fragmented medio-ventral ridge, PhC. Scale bars: A = 20 μm; B–H = 10 μm.

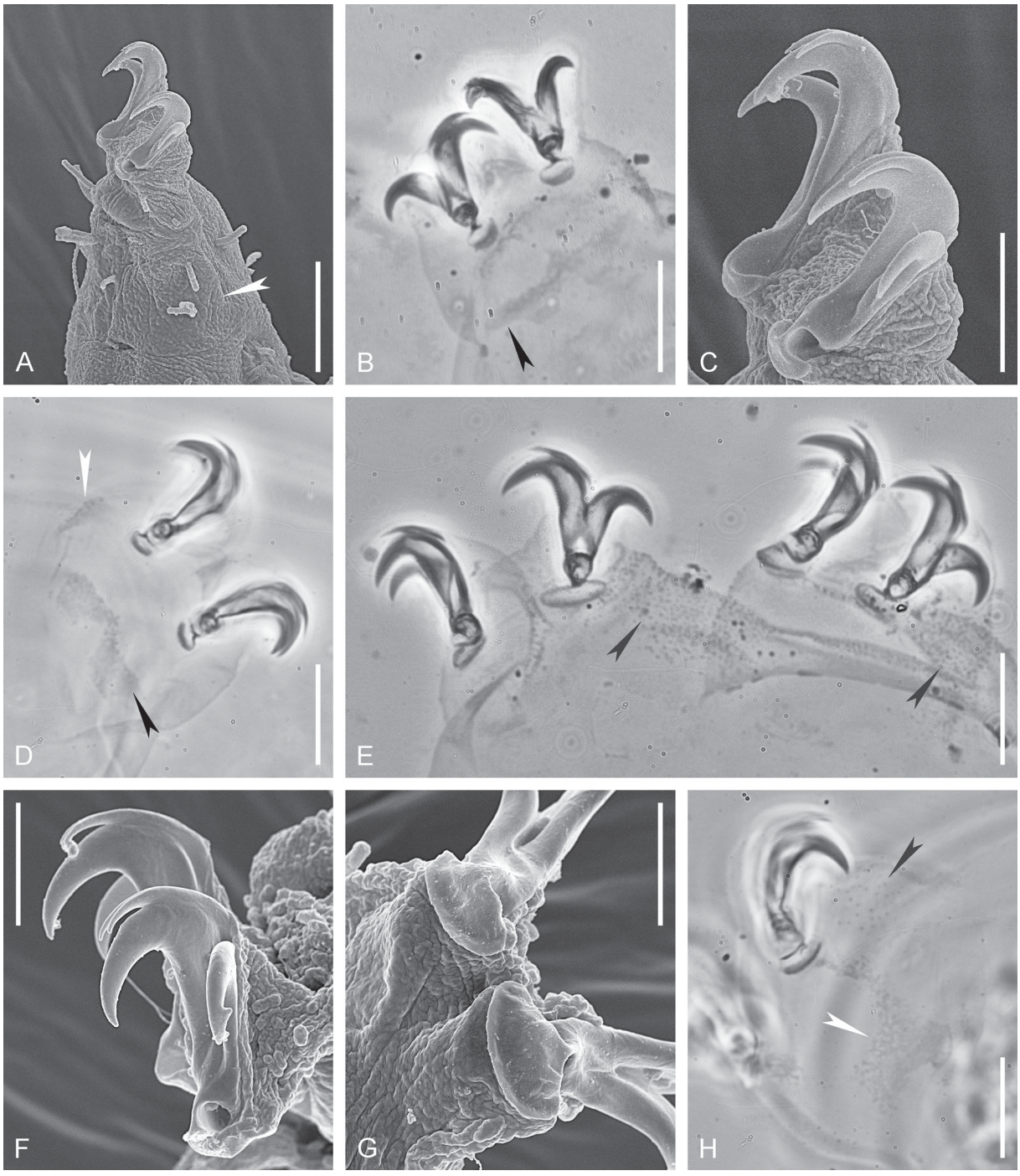

Fig. 10. *Mesobiotus vulpinus* sp. nov., claws. **A, C, F–G**. Paratype (SPbU Tar_33). **B**. Paratype (SPbU 320(1)). **D, H**. Holotype (SPbU 320(10)). **E**. Paratype (SPbU 320(5)). **A**. Inner surface of leg III, white arrowhead indicates indistinctly marked pulvinus, SEM. **B**. Claws of leg II, black arrowhead indicates bar-like cuticular thickening, PhC. **C**. Claws of leg III, SEM. **D**. Claws of leg I, focused on bar-like cuticular thickening, black arrowhead, white arrowhead indicates the zone of dot-like sculpture, PhC. **E**. Claws of leg IV, black arrowheads indicate cuticular sculpture around the claw bases, PhC. **F**. Claws of leg IV, SEM. **G**. Lunules of claws of leg IV, SEM. **H**. Leg IV, focused on horseshoe-like structure, white arrowhead, black arrowhead indicates cuticular sculpture around the claw base, PhC. Scale bars: A–B, D–E, H = 10 μm; C, F–G = 5 μm.

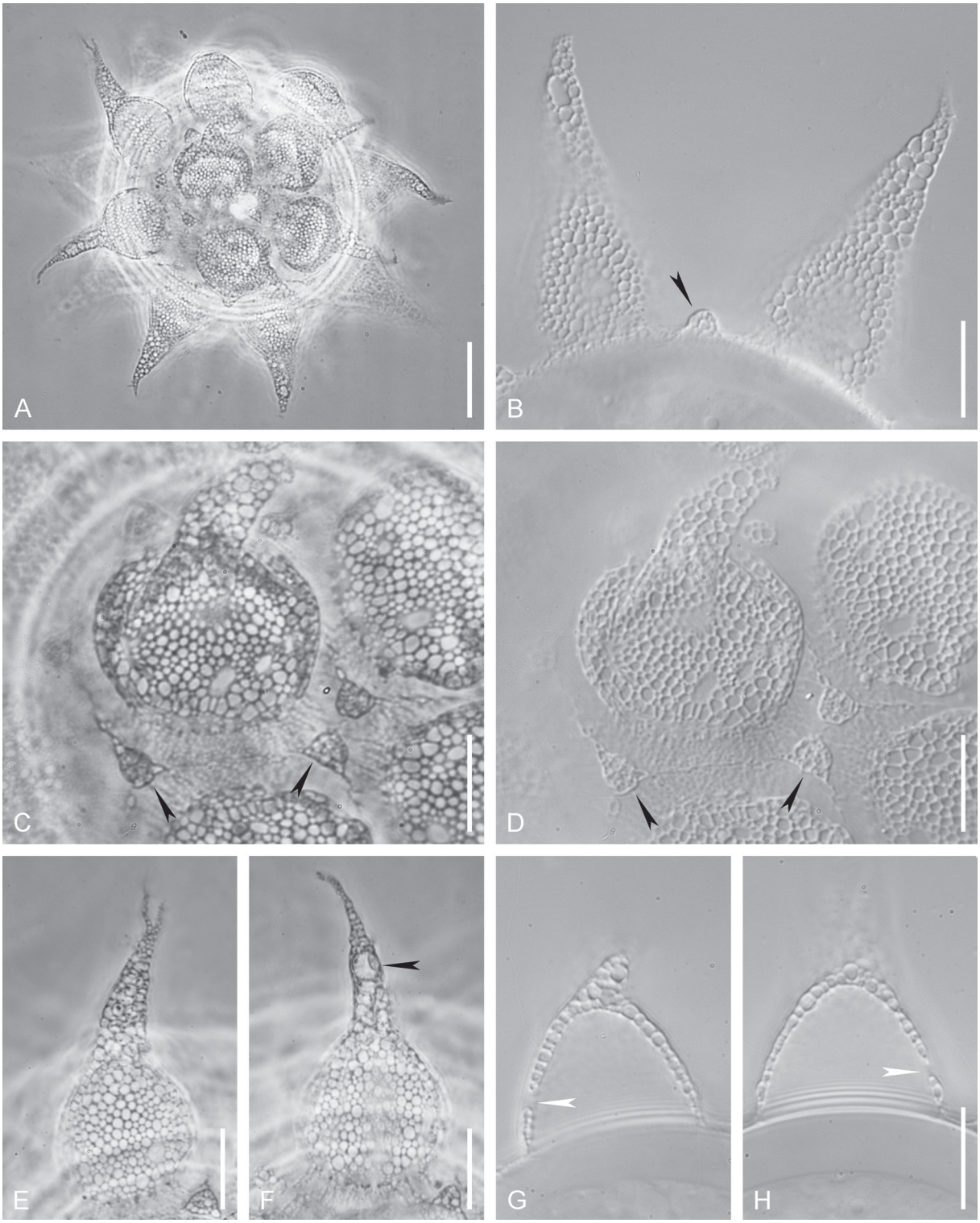

Fig. 11. *Mesobiotus vulpinus* sp. nov., paratype (SPbU 320(6)), egg. **A**. Total view of the egg, PhC. **B**. Egg processes with small bulbous process between them, black arrowhead, DIC. **C–D**. Details of the egg surface, black arrowheads indicate small bulbous processes, PhC (C), DIC (D). **E**. Bifurcated egg process, PhC. **F**. Egg process with "bubble", black arrowhead, PhC. **G–H**. Optical sections of the egg process basal part, white arrowheads indicate a pore, DIC. Scale bars: A = 20 μm; B–H = 10 μm.

Table 5. Measurements (in µm) of selected morphological structures of eggs of *Mesobiotus vulpinus* sp. nov. Abbreviations: N = number of eggs/structures measured, range refers to the smallest and the largest structure among all measured specimens; SD = standard deviation).

CHARACTER	N	RANGE	MEAN	SD
Egg bare diameter	3	66,2 – 67,3	66,7	0,6
Egg full diameter	3	125,4 – 131,0	128,8	3,0
Process height	9	29,8 – 36,1	33,0	2,4
Process base width	9	15,9 – 19,0	18,0	0,9
Process base/height ratio	9	50% – 63%	55%	4%
Inter-process distance	9	2,0 – 7,4	5,0	1,9
Number of processes on the egg circumference	3	9 – 9	9,0	0,0

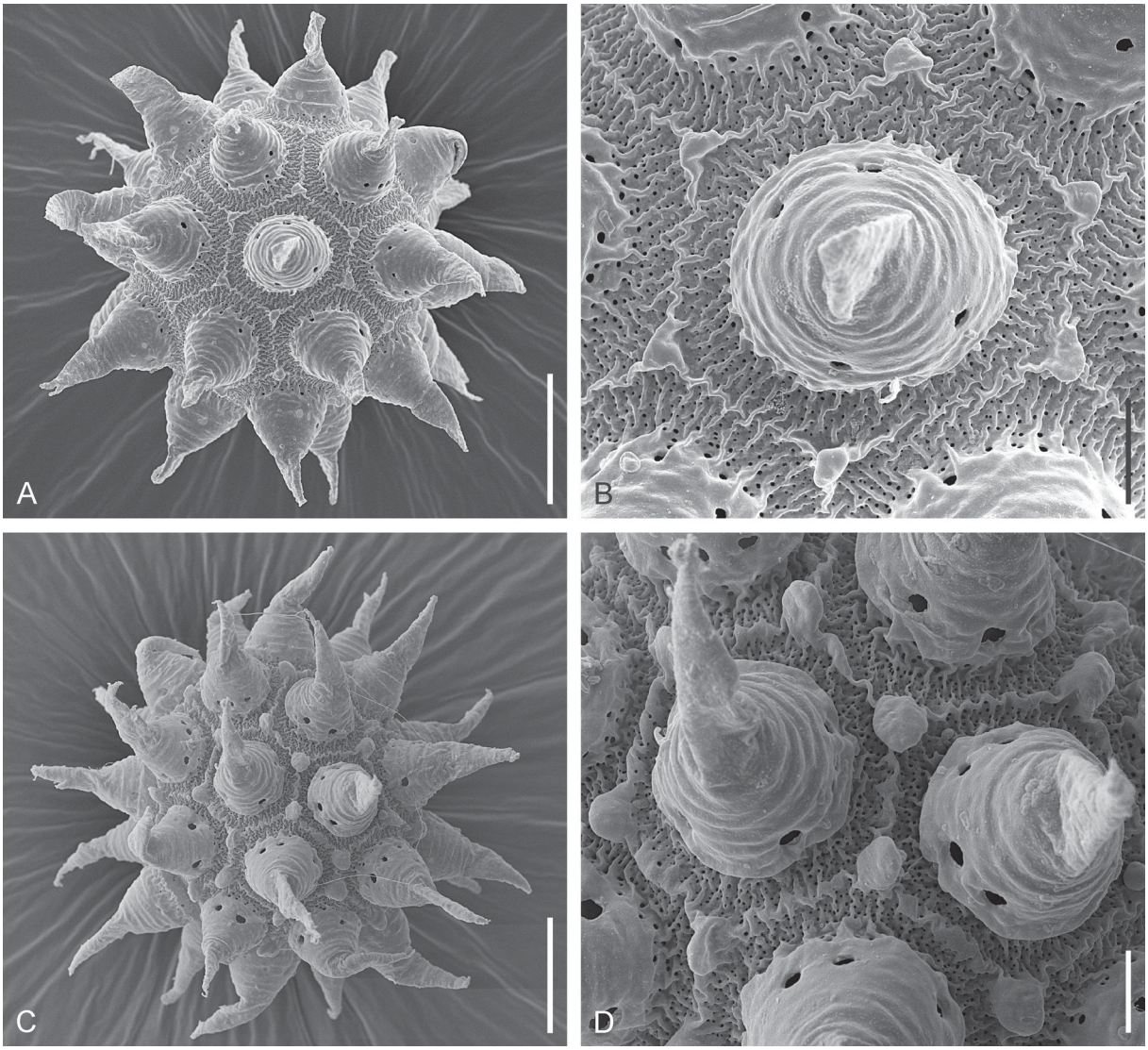

Fig. 12. *Mesobiotus vulpinus* sp. nov., egg. **A–D**. Paratypes (SPbU Tar_65). **A, C**. Total view of the eggs, SEM. **B, D**. Details of the egg surface, SEM. Note the difference in the degree of development of small tubercles and numerous small pores on the egg surface. Scale bars: A–B = 20 µm; C–D = 5 µm.

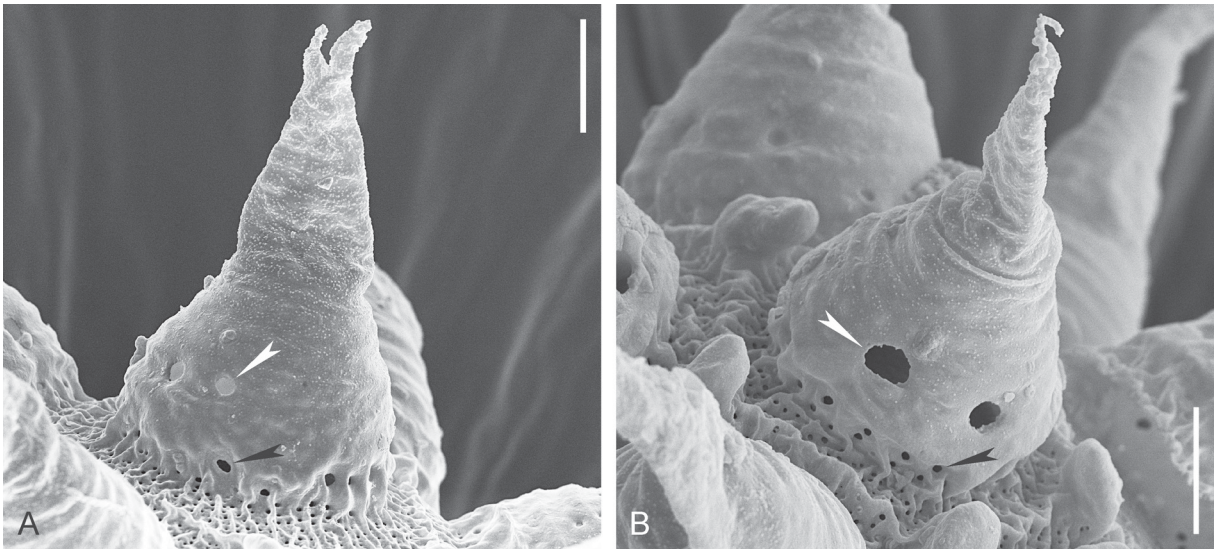

Fig. 13. *Mesobiotus vulpinus* sp. nov., paratype (SPbU Tar_65), egg. **A–B**. Details of the egg processes, whire arrowheads indicate large pores, black arrowheads indicate small pores, SEM. Scale bars = 5 μm.

DNA sequences

Sequences for all four molecular markers were obtained from two specimens (18S rRNA – OR804461, OR804462, 28S rRNA – OR805140, OR805141, ITS-2 – OR805172, OR805173, COI – OR803040, OR803041; voucher slides SpbU 320(08) and 320(15))

Discussion

Phenotypic differential diagnosis of *Mesobiotus efa* sp. nov.

Within the genus, *Mesobiotus efa* sp. nov. belongs to the group of species with smooth cuticle, *harmsworthi*-type OCA, typical *Mesobiotus* claws IV with unindented lunules, and egg chorion with reticulated processes in form of "sharp wide cones" or "cones with long slender endings" (these two types of processes are often poorly distinguishable), egg process bases with well-developed crone of dark thickenings without finger-like projections, and egg shell surface between the processes with ridges without reticulation, areolation or semi-areolation.

Within this species complex *Mesobiotus efa* sp. nov. differs from:

Mesobiotus altitudinalis (known only from the type locality in Russia; Biserov 1997–1998) by having typical *Mesobiotus* claws while *M. altitudinalis* has thin elongated claws, especially on legs IV, by having numerous additional teeth in OCA ventrally, by having eggs with smaller egg processes (processes height 11.1–21.6 μm in *M. efa* sp. nov. vs 22.0–35.0 μm in *M. altitudinalis*), and by having egg surface between processes without pores.

Mesobiotus baltatus (McInnes, 1991) (known only from the type locality in Spain; McInnes 1991) by having no pigmented bands (present in *M. baltatus*) and by having well-developed crone of dark thickenings around the egg processes (absent in *M. baltatus*).

Mesobiotus binieki (Kaczmarek, Gołdyn, Prokop & Michalczyk, 2011) (known only from the type locality in Bulgaria; Kaczmarek *et al.* 2011) by having medio-ventral ridges of OCA always unbroken, and by having egg processes with less differentiated basal and apical parts (in *M. binieki* the basal parts

are in shape of very short and wide cones while the apical parts are long thin spines without developed internal bubbles.

Mesobiotus coronatus (de Barros, 1942) (with certainty known from South America only; Pilato *et al.* 2000; Kaczmarek *et al.* 2015) by having shorter claws (*pt* for anterior/posterior claws of legs IV are 16.8–27.5/22.4–29.0 in *M. efa* sp. nov. and 27.3–30.5/30.6–32.6 in *M. coronatus*), and by having larger eggs (egg diameter without processes is 67.5–69.1 µm in *M. efa* and 42–55 µm in *M. coronatus*) with larger processes (process height is 11.1–21.6 µm in *M. efa* and up to 9.2 µm in *M. coronatus*).

Mesobiotus emiliae Massa, Guidetti, Cesari, Rebecchi & Jönsson, 2021 (known only from the type locality in Sweden; Massa *et al.* 2021), by having slightly larger eggs (egg diameter without processes is 67.5–69.1 µm in *M. efa* sp. nov. and 46.9–64.6 µm in *M. emiliae*) with higher egg processes (process height is 11.1–21.6 µm in *M. efa* and 7.9–10.6 µm in *M. emiliae*), by having egg processes with relatively longer apical parts, and by having larger inter-process distances (2.2–6.6 µm in *M. efa* and 0.5–1.6 µm in *M. emiliae*).

Mesobiotus helenae Tumanov & Pilato, 2019 (known only from the type locality in New Zealand; Tumanov & Pilato 2019) by having medio-ventral ridges of OCA always unbroken (divided in *M. helenae*), having shorter claws (*pt* for posterior claws of legs IV are 22.4–29.0 in *M. efa* sp. nov. and 30.7–31.4 in *M. helenae*), and by having smaller eggs (egg diameter without processes is 67.5–69.1 µm in *M. efa* and 71.0 µm in *M. helenae*) with less numerous processes (number of processes on the egg circumference is 12–14 in *M. efa* and 22 in *M. helenae*), and processes walls with well-developed internal reticulation (poorly visible in *M. helenae*).

Mesobiotus insuetus (Pilato, Sabella & Lisi, 2014) (known only from the type locality in Sicily, Italy; Pilato *et al.* 2014) by having lower *pt* value for stylet supports insertion point (74.0–78.8 in *M. efa* sp. nov. and 79.0–79.4 in *M. insuetus*), by having shorter macroplacoid row (*pt* value 31.3–45.3 in *M. efa* and 46.2–48.9 in *M. insuetus*), by having claws of legs I–III and legs IV similar (claws of legs IV are markedly different in *M. insuetus*), and by having higher egg processes (process height is 11.1–21.6 µm in *M. efa* and 7.9–8.6 µm in *M. insuetus*).

Mesobiotus imperialis Stec, 2021 (known only from the type locality in Vietnam; Stec 2021) by having medio-ventral ridges of OCA always unbroken (divided in *M. imperialis*), by having lunules on legs IV always smooth (slight indentation visible in about 50% of observed specimens of *M. imperialis*), by having egg surface between processes without pores (in *M. imperialis* pores are present and visible in LM as light dots), and by having a single row of large pores around the smooth egg processes (in *M. imperialis* egg processes with numerous depressions and pores not organised in rows) – the last character detectable in SEM only.

Mesobiotus nikolaevae Tumanov, 2018 (known only from the type locality in Croatia; Tumanov 2018b) by having more numerous additional teeth in ventral OCA, by having egg surface between processes without pores (in *M. nikolaevae* pores are present and visible in LM as light dots), by having ridges between egg processes poorly visible in LM (well-developed, forming a reticulate-like pattern in *M. nikolaevae*), and by having a single row of large pores around the egg processes (in *M. nikolaevae* egg processes with irregularly distributed small pores) – the last character detectable in SEM only.

Mesobiotus occultatus Kaczmarek, Zawierucha, Buda, Stec, Gawlak, Michalczyk & Roszkowska, 2018 (known only from Spitsbergen; Kaczmarek *et al.* 2018) by having medio-ventral ridges of OCA always unbroken (often divided in *M. occultatus*, the character not mentioned in the original description (Kaczmarek pers. com. 2 Nov. 2019)), by having eggs with less tightly distributed processes (inter-process distance is 2.2–6.6 µm (mean 4.4 µm) in *M. efa* sp. nov. and 1.4–4.2 µm (mean 2.6 µm) in

M. occultatus), and by having a single row of large pores around the egg processes (smaller pores, less regularly distributed over the processes in *M. occultatus*).

Mesobiotus patiens (Pilato, Binda, Napolitano & Moncada, 2000) (known from the Aeolian Islands (type locality) and several islands in the Tyrrhenian Sea, Italy; Pilato *et al.* 2000) by having numerous additional teeth in ventral OCA (no such teeth in *M. patiens*), and by having smaller eggs (egg diameter without processes is 67.5–69.1 µm in *M. efa* sp. nov. and 75–87 µm in *M. patiens*) with distal part of the processes better developed with well-visible internal bubbles (in *M. patiens* distal part of the processes reduced, thin and short, often broken, without internal bubbles).

Mesobiotus rigidus (Pilato & Lisi, 2006) (known only from the type locality in New Zealand; Pilato & Lisi 2006) by having eggs with system of radial ridges on the egg shell surface between processes poorly visible in LM (well-visible in *M. rigidus*) and presence of bifurcated processes and tuft of short filaments on the processes' top (egg processes never subdivided in *M. rigidus*).

Genetic comparison of *Mesobiotus efa* sp. nov.

The ranges of uncorrected genetic *p*-distances between the studied population of *Mesobiotus efa* sp. nov. and other species of the genus *Mesobiotus*, for which sequences are available from GenBank, are as follows:

COI: 20.33%–33.84% (mean 27.14%), with the most similar being *M. occultatus* from Svalbard (MH195152, Kaczmarek *et al.* 2018), and the least similar being *M. dilimanensis* Itang, Stec, Mapalo, Mirano-Bascos & Michalczyk, 2020 from the Philippines (MN257047, Itang *et al.* 2020).

18S rRNA: 0.31%–6.44% (mean 3.96%), with the most similar being *M. occultatus* (OR794157, this work), and the least similar being *M.* cf. *furciger* from Antarctica (MW751947, Short *et al*. 2022).

28S rRNA: 0.96%–14.56% (mean 6.09%), with the most similar being *M. occultatus* (OR794158, this work), and the least similar being *M. dilimanensis* (MN257049, Itang *et al*. 2020).

ITS-2: 4.78%–54.74% (mean 26.71%), with the most similar being *M. occultatus* (MH197155, Kaczmarek *et al.* 2018; OR805249, this work), and the least similar being *M. marmoreus* Stec, 2021 from Vietnam (OL257861–OL257863, Stec 2021).

Full matrices with *p*-distances are provided in the Supp. file 6.

Phenotypic differential diagnosis of *Mesobiotus vulpinus* sp. nov.

Within the genus *Mesobiotus* only *M. mauccii* (Pilato, 1974) (described from South China; Pilato 1974) has egg chorion with polygonal relief. *Mesobiotus vulpinus* sp. nov. differs from *M. mauccii* by having eyes, by having narrower buccal tube (*pt* for the buccal tube external width is 13.0–18.2 in *M. vulpinus* and 23.12 in *M. mauccii* (buccal tube measurements was taken from the type specimen photo), by having stylet supports inserted in more anterior position (*pt* for the stylet support insertion point is 74.7–77.6 in *M. vulpinus* and 79.49 in *M. mauccii*, by having no additional teeth in dorsal OCA and only few additional teeth in ventral OCA (*M. mauccii* has additional teeth both in dorsal and ventral OCA, ventral additional teeth are numerous and organized in several rows), by having longer egg processes (29.8–36.1 µm in *M. vulpinus* and 15–19 µm in *M. mauccii*) with less differentiated basal and apical parts, by lack of collar around the process base, and by usually evidently developed small bulbous processes in the intersection points of polygonal relief ridges (Fig. 12C–D) (intersection points with poorly developed thickenings in *M. mauccii*: "the vertices of these polygons are particularly prominent and almost form a tubercle" (Pilato 1974: 67). Rarely in some eggs of *M. vulpinus* these processes are small, similar to those in *M. mauccii* (Fig. 12A–B).

Mesobiotus mauccii was also noted from several Asian locations: North China (Beasley & Miller 2007), Central China (Beasley & Miller 2012), South Andaman Island (Maucci & Durante Pasa 1980), and Japan (Utsugi 1988; Abe & Takeda 2000; Abe & Takeda 2005). All China records mostly conform to the original description of *M. mauccii*, while in Abe & Takeda's (2005) photographs egg processes are longer and evidently different in shape, being more similar to the *M. vulpinus* sp. nov. egg processes. Also the buccal tube seems to be narrower in Japanese specimens than in type material of *M. mauccii* (see Abe & Takeda 2005: fig. 3) and eyes are present, like in *M. vulpinus*. In our opinion, it is very likely that the Japanese records of *M. mauccii* are in fact *M. vulpinus* or a similar species. The Andaman record is the most questionable as the photograph of an adult specimen attributed to *M. mauccii* in Maucci & Durante Pasa (1980) in fact belongs to an unknown species of *Paramacrobiotus* (see Abe & Takeda 2000) and the only evidence of the presence of this species on the Andaman Islands is the photo of a damaged egg.

Genetic comparison of *Mesobiotus vulpinus* sp. nov.

The ranges of uncorrected genetic *p*-distances between the studied population of *Mesobiotus vulpinus* sp. nov. and other species of the genus *Mesobiotus*, for which sequences are available from GenBank, are as follows:

COI: 24.60%–33.03% (mean 29.61%), with the most similar being *M. diegoi* Stec, 2022 from South Africa (OP143857, OP143858, Stec 2022), and the least similar being *M. dilimanensis* from the Philippines (MN257047, Itang *et al.* 2020).

18S rRNA: 0.21%–5.92% (mean 3.33%), with the most similar being *M. occultatus* (OR794157, this work), and the least similar being *M.* cf. *furciger* from Antarctica (MW751947, Short *et al*. 2022).

28S rRNA: 3.38%–14.37% (mean 6.21%), with the most similar being *M. efa* sp. nov. (OR805135–OR805139, this work), and the least similar being *M. dilimanensis* (MN257049, Itang *et al*. 2020).

ITS-2: 15.94%–51.77% (mean 27.49%), with the most similar being *Mesobiotus* gr. *harmsworthi* from Russia (MH197157, Kaczmarek *et al.* 2020), and the least similar being *M. marmoreus* from Vietnam (OL257861–OL257863, Stec 2021).

Full matrices with *p*-distances are provided in the Supp. file 6.

Phylogenetic analysis

General topology of the obtained consensus phylogenetic tree (Fig. 14) conforms to the results of the most recent analyses performed by Stec (2022) and Vecchi *et al.* (2023). The monophyletic genus *Mesobiotus* comprises a complex of basal Antarctic clades paraphyletic in both Bayesian, and ML analyses consisted of two clearly separated subclades: the first incorporates *M. hilariae* Vecchi, Cesari, Bertolani, Jönsson, Rebecchi & Guidetti, 2016 and undescribed species of *M. harmsworthi* morphogroup (Short *et al.* 2022) and the second incorporates at least four well-supported subclades of undescribed species of *M. furciger* morphogroup (Short *et al.* 2022; morphogroups according Stec 2022).

The second main subclade, which incorporates all non-Antarctic taxa, revealed monophyletic in our analysis, but with weak support (0.85 in Bayes and 76 in ML). This is in contrast with the results of Stec (2022), where the high support for the monophyly of this clade was obtained. This clade consists of two monophyletic clades: the first comprising two South Asian species (*M. dilimanensis* from the Philippines and *M. marmoreus* from Vietnam) and the second including all other species of *Mesobiotus*. This second subclade incorporates a larger subclade consisting of two distinct species complexes: the first including Holarctic species and the second including mostly tropical or subtropical

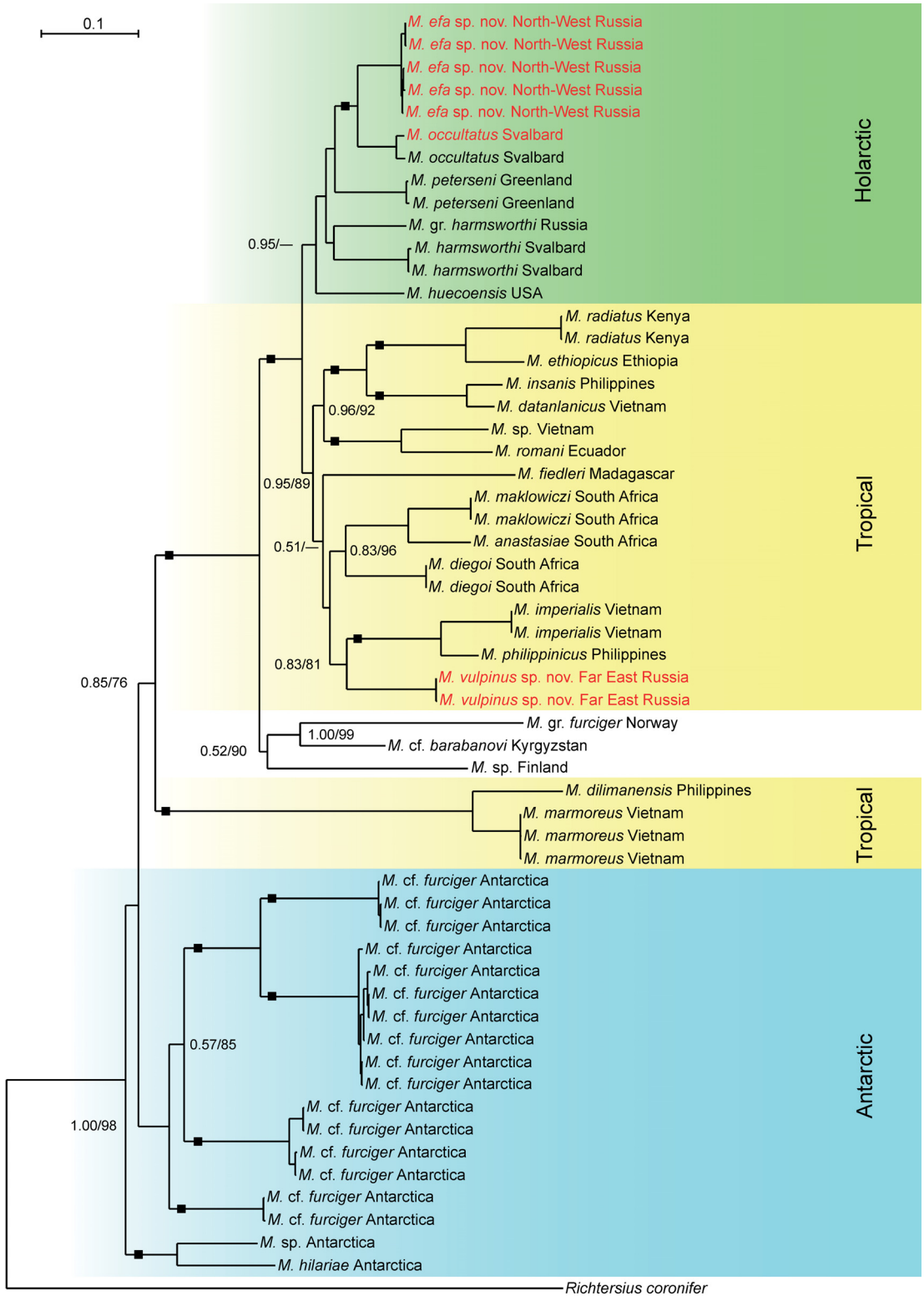

Fig. 14. Phylogeny of *Mesobiotus* Vecchi, Cesari, Bertolani, Jönsson, Rebecchi & Guidetti, 2016 based on concatenated 18S+28S+ITS-2+COI sequences. Numbers at nodes indicate Bayesian posterior probability values (BI, first values) and bootstrap values (ML, second values). Black dots indicate the nodes supported by values of 1.0/100% with both methods. Low support values (below 0.9 in BI and below 70% in ML) not shown. Scale bar and branch lengths refer to the Bayesian analysis.

species. Sister group to this "Holarctic +Tropical" subclade is a small subclade, consisting of only three species (*M.* cf. *barabanovi* from Kyrgyzstan, *M.* gr. *furciger* from Norway, and *Mesobiotus* sp. from Finland). The Holarctic subclade includes *M. huecoensis* from USA, *M. peterseni* from Greenland, *M. harmsworthi* from Svalbard, *M.* gr. *harmsworthi* from Russia and the monophyletic clade comprises *M. occultatus* from Svalbard and *M. efa* sp. nov. from North-West Russia as sister groups. The position of *M. huecoensis* is instable – in the Bayesian analysis it is a sister group to all other (North Holarctic) species of the subclade, while in the ML analysis it is a sister group to *M. peterseni* (with weak support, 67%). Such ambiguity can be the result of the data incompleteness for this species: only 18S rRNA and COI sequences are available.

The most notable differences from the results of previous studies relate to the structure of a relatively large 'tropical' species complex. Within this clade, we obtained three moderately- to well-supported subclades with poorly resolved relationships between them. For the first time, we state the presence of a moderately-supported monophyletic clade comprising all known South African species (*M. anastasiae* Tumanov, 2020, *M. maklowiczi* Stec, 2022, and *M. diegoi* Stec, 2022). The second clade consists of Asian species (*M. imperialis* Stec, 2021 from Vietnam, *M. philippinicus* Mapalo, Stec, Mirano-Bascos & Michalczyk, 2016 from the Philippines, and *M. vulpinus* sp. nov. from Russian Far East. Madagascaran species *M. fiedleri* Kaczmarek, Bartylak, Stec, Kulpa, M. Kepel, A. Kepel & Roszkowska, 2020 has instable position being related to these two clades in the Bayesian analysis, although with weak support (0.51), while in the ML analysis it is a sister group to the South African species complex also with weak support (58%).

The third clade incorporates three subclades: African (*M. ethiopicus* Stec & Kristensen, 2017 from Ethiopia + *M. radiatus* (Pilato, Binda & Catanzaro, 1991) from Kenya) and South Asian (*M. datanlanicus* Stec, 2019 from Vietnam + *M. insanis* Mapalo, Stec, Mirano-Bascos & Michalczyk, 2017 from the Philippines) as sister groups, and *M. romani* Roszkowska, Stec, Gawlak & Kaczmarek, 2018 from Ecuador + *Mesobiotus* sp. from Vietnam related to them.

It is interesting to note presence of three independent clades consisting of species from Vietnam and the Philippines: *M. dilimanensis* + *M. marmoreus*; *M. imperialis* + *M. philippinicus*, and *M. datanlanicus* + *M. insanis*. Such a zoogegraphic pattern can be evidence for the strong ancient connections between tardigrade faunas of these regions. A close relationship of the newly described species from the Russian Far East (Primorsky Krai) to one of the South Asian clades is not surprising. The presence of tropical elements in the invertebrate fauna of Primorsky Krai is a well-known phenomenon (Likharev 1953; Korovchinsky 2006; Markova *et al*. 2015; Ganin 2018; Garibian 2020). This region is usually considered as a refugium of the Neogene tropical fauna escaping the influence of the last glaciation (Likharev 1953). The morphological similarity of *M. vulpinus* sp. nov. to *M. maucchii*, known from China and, possibly, the Andaman Islands supports its close affinity to the tropical species complex.

Acknowledgements

We would like to thank Prof. G. Pilato (University of Catania, Italy) and Prof. R. Bertolani for providing the photographs of the type specimen of *Mesobiotus mauccii*. This study was carried out with the use of the equipment of the Core Facilities Centers: "Culture Collection of Microorganisms" and "Centre for Molecular and Cell Technologies" of the St Petersburg State University. The study was supported by the Russian Science Foundation grant № 23-24-00201 "Study of the fauna of terrestrial tardigrades in Russia", https://rscf.ru/en/project/23-24-00201/.

References

Abe W. & Takeda M. 2000. Tardigrades from the Imperial Palace, Tokyo. *Memoirs of the National Science Museum Tokyo* 35: 165–177.

Abe W. & Takeda M. 2005. Semiterrestrial tardigrades from the Tokiwamatsu Imperial Villa, Tokyo, Japan. *Memoirs of the National Science Museum Tokyo* 39: 503–510.

Beasley C.W. & Miller W.R. 2007. Tardigrada of Xinjiang Uygur Autonomous Region, China. *Journal of Limnology* 66 (1s): 49–55. https://doi.org/10.4081/jlimnol.2007.s1.49

Beasley C.W. & Miller W.R. 2012. Additional Tardigrada from Hubei Province, China, with the description of *Doryphoribius barbarae* sp. nov. (Eutardigrada: Parachela: Hypsibiidae). *Zootaxa* 3170: 55–63. https://doi.org/10.11646/zootaxa.3170.1.5

Bertolani R., Cesari M., Giovannini I., Rebecchi L., Guidetti R., Kaczmarek Ł. & Pilato G. 2023. The *Macrobiotus persimilis-polonicus* complex (Eutardigrada, Macrobiotidae), another example of problematic species identification, with the description of four new species. *Organisms Diversity & Evolution* 23: 329–368. https://doi.org/10.1007/s13127-022-00599-z

Biserov V.I. 1991. An annotated list of Tardigrada from European Russia. *Zoologische Jahrbücher. Abteilung für Anatomie und Ontogenie der Tiere* 118: 193–216.

Biserov V.I. 1996. Tardigrades of the Taimyr Peninsula with description of two new species. *Zoological Journal of the Linnean Society* 116: 215–237. https://doi.org/10.1111/j.1096-3642.1996.tb02345.x

Biserov V. I. 1997–1998. Tardigrades of the Caucasus with a taxonomic analysis of the genus *Ramazzottius* (Parachela: Hypsibiidae). *Zoologischer Anzeiger* 236: 139–159.

Degma P. & Guidetti R. 2023. *Actual checklist of Tardigrada species*. https://doi.org/10.25431/11380_1178608 [accessed 11 Oct. 2023].

Ganin G.N. 2018. New data on the *Drawida* (Moniligastridae) tropical earthworms at their northern habitat edge. *Vestnik DVO RAN* 2018 (4): 49–56 [In Russian.]

Garibian P.G. 2020. *Fauna of Cladoceran Crustaceans (Crustacea: Cladocera) South of the Far East of the Russian Federation and Korean Peninsula.* PhD Dissertation, A.N. Severtsov Institute of Ecology and Evolution of the Russian Academy of Sciences. [In Russian.]

Gouy M., Guindon S. & Gascuel O. 2010. SeaView version 4: a multiplatform graphical user interface for sequence alignment and phylogenetic tree building. *Molecular Biology and Evolution* 27 (2): 221–224. https://doi.org/10.1093/molbev/msp259

Guidetti R., Cesari M., Bertolani R., Altiero T. & Rebecchi L. 2019. High diversity in species, reproductive modes and distribution within the *Paramacrobiotus richtersi* complex (Eutardigrada, Macrobiotidae). *Zoological Letters* 5: 1. https://doi.org/10.1186/s40851-018-0113-z

Itang L.A.M., Stec D., Mapalo M.A., Mirano-Bascos D. & Michalczyk Ł. 2020. An integrative description of *Mesobiotus dilimanensis*, a new tardigrade species from the Philippines (Eutardigrada: Macrobiotidae: *furciger* group). *Raffles Bulletin of Zoology* 68: 19–31.

Kaczmarek Ł. & Michalczyk Ł. 2017. The *Macrobiotus hufelandi* group (Tardigrada) revisited. *Zootaxa* 4363 (1): 101. https://doi.org/10.11646/zootaxa.4363.1.4

Kaczmarek Ł., Gołdyn B., Prokop Z.M. & Michalczyk Ł. 2011. New records of Tardigrada from Bulgaria with the description of *Macrobiotus binieki* sp. nov. (Eutardigrada: Macrobiotidae) and a key to the species of the *harmsworthi* group. *Zootaxa* 2781 (1): 29–39. https://doi.org/10.11646/zootaxa.2781.1.2

Kaczmarek Ł., Cytan J., Zawierucha K., Diduszko D. & Michalczyk Ł. 2014. Tardigrades from Peru (South America), with descriptions of three new species of Parachela. *Zootaxa* 3790 (2): 357–379. https://doi.org/10.11646/zootaxa.3790.2.5

Kaczmarek Ł., Michalczyk Ł. & McInnes S.J. 2015. Annotated zoogeography of non-marine Tardigrada. Part II: South America. *Zootaxa* 3923 (1): 1–107. https://doi.org/10.11646/zootaxa.3923.1.1

Kaczmarek Ł., Gawlak M., Bartels P.J., Nelson D.R. & Roszkowska M. 2017. Revision of the genus *Paramacrobiotus* Guidetti *et al*., 2009 with the description of a new species, re-descriptions and a key. *Annales Zoologici* 67 (4): 627–656. https://doi.org/10.3161/00034541ANZ2017.67.4.001

Kaczmarek Ł., Zawierucha K., Buda J., Stec D., Gawlak M., Michalczyk Ł. & Roszkowska M. 2018. An integrative redescription of the nominal taxon for the *Mesobiotus harmsworthi* group (Tardigrada: Macrobiotidae) leads to descriptions of two new *Mesobiotus* species from Arctic. *PLoS ONE* 13 (10): e0204756. https://doi.org/10.1371/journal.pone.0204756

Kaczmarek Ł., Bartylak T., Stec D., Kulpa A., Kepel M., Kepel A. & Roszkowska M. 2020. Revisiting the genus *Mesobiotus* Vecchi *et al*., 2016 (Eutardigrada, Macrobiotidae) – remarks, updated dichotomous key and an integrative description of new species from Madagascar. *Zoologischer Anzeiger* 287: 121–146. https://doi.org/10.1016/j.jcz.2020.05.003

Kaczmarek Ł., Rutkowski T., Zacharyasiewicz M., Surmacki A., Osiejuk T.S. & Hayastha P. 2023. New species of Macrobiotidae (Eutardigrada) from Cameroon (Africa), characteristics of *Macrobiotus* morpho-groups and a key to the *nelsonae* group. *Annales Zoologici* 73: 1–15. https://doi.org/10.3161/00034541ANZ2023.73.1.001

Kalyaanamoorthy S., Minh B.Q., Wong T.K.F., von Haeseler A. & Jermiin L.S. 2017. ModelFinder: fast model selection for accurate phylogenetic estimates. *Nature Methods* 14: 587–589. https://doi.org/10.1038/nmeth.4285

Katoh K., Misawa K., Kuma K. & Miyata T. 2002. MAFFT: a novel method for rapid multiple sequence alignment based on fast Fourier transform. *Nucleic Acids Research* 30: 3059–3066. https://doi.org/10.1093/nar/gkf436

Kiosya Y., Pogwizd J., Matsko Y., Vecchi M. & Stec D. 2021. Phylogenetic position of two *Macrobiotus* species with a revisional note on *Macrobiotus sottilei* Pilato, Kiosya, Lisi & Sabella, 2012 (Tardigrada: Eutardigrada: Macrobiotidae). *Zootaxa* 4933 (1): 113–135. https://doi.org/10.11646/zootaxa.4933.1.5

Korovchinsky N.M. 2006. The Cladocera (Crustacea: Branchiopoda) as a relict group. *Zoological Journal of the Linnean Society* 147: 109–124. https://doi.org/10.1111/j.1096-3642.2006.00217.x

Larsson A. 2014. AliView: a fast and lightweight alignment viewer and editor for large data sets. *Bioinformatics* 30 (22): 3276–3278. https://doi.org/10.1093/bioinformatics/btu531

Likharev I.M. 1953 Features of the distribution of mollusks in Primorsky Krai. *Trudy Zoologicheskogo Instituta Academii Nauk SSSR* 13: 277–288. [In Russian.]

Mapalo M., Stec D., Mirano-Bascos D.M. & Michalczyk Ł. 2016. *Mesobiotus philippinicus* sp. nov., the first limnoterrestrial tardigrade from the Philippines. *Zootaxa* 4126 (3): 411–426. https://doi.org/10.11646/zootaxa.4126.3.6

Mapalo M., Stec D., Mirano-Bascos D. & Michalczyk Ł. 2017. An integrative description of a limnoterrestrial tardigrade from the Philippines, *Mesobiotus insanis*, new species (Eutardigrada: Macrobiotidae: *harmsworthi* group). *Raffles Bulletin of Zoology* 65: 440–454.

Markova T.O., Repsh N.V. & Maslov M.V. 2015. The arealogical analysis of the dipteran fauna (Diptera: Tachinidae, Phasiinae) in the South Primorye. *The Bulletin of KrasGAU* 2015 (5): 27–30. [In Russian.]

Massa E., Guidetti R., Cesari M., Rebecchi L. & Jönsson K.I. 2021. Tardigrades of Kristianstads Vattenrike Biosphere Reserve with description of four new species from Sweden. *Scientific Reports* 11: 4861. https://doi.org/10.1038/s41598-021-83627-w

Maucci W. & Durante Pasa M.V. 1980. Tardigradi muscicoli delle Isole Andamane. *Bollettino del Museo Civico di Storia Naturale di Verona* 7: 281–291.

McInnes S.J. 1991. Notes on tardigrades from the Pyrenees, including one new species. *Pedobiologia* 35: 11–26. https://doi.org/10.1016/S0031-4056(24)00040-4

Michalczyk Ł. & Kaczmarek Ł. 2003. A description of the new tardigrade *Macrobiotus reinhardti* (Eutardigrada: Macrobiotidae, *harmsworthi* group) with some remarks on the oral cavity armature within the genus *Macrobiotus* Schultze. *Zootaxa* 331: 1–24. https://doi.org/10.11646/zootaxa.331.1.1

Michalczyk Ł. & Kaczmarek Ł. 2013. The Tardigrada Register: a comprehensive online data repository for tardigrade taxonomy. *Journal of Limnology* 72 (s1): e22. https://doi.org/10.4081/jlimnol.2013.s1.e22

Miller M.A., Pfeiffer W. & Schwartz T. 2010. Creating the CIPRES Science Gateway for inference of large phylogenetic trees. *Gateway Computing Environments Workshop (GCE)*: 1–8. https://doi.org/10.1109/GCE.2010.5676129

Minh B.Q., Schmidt H.A., Chernomor O., Schrempf D., Woodhams M.D., von Haeseler A. & Lanfear R. 2020. IQ-TREE 2: New models and efficient methods for phylogenetic inference in the genomic era. *Molecular Biology and Evolution* 37: 1530–1534. https://doi.org/10.1093/molbev/msaa015

Morek W., Stec D., Gąsiorek P., Schill R.O., Kaczmarek Ł. & Michalczyk Ł. 2016. An experimental test of eutardigrade preparation methods for light microscopy. *Zoological Journal of the Linnean Society* 178 (4): 785–793. https://doi.org/10.1111/zoj.12457

Nelson D.R., Bartels P.J. & Guil N. 2018. Tardigrade ecology. *In*: Schill R.O. (ed.) *Water Bears: The Biology of Tardigrades*. *Zoological Monographs* 2: 163–210. Springer Nature Switzerland AG. https://doi.org/10.1007/978-3-319-95702-9_7

Pilato G. 1974. Tre nouve specie di Tardigradi muscicoli di Cina. *Animalia* 1: 59–68.

Pilato G. 1981. Analisi di nuovi caratteri nello studio degli Eutardigradi. *Animalia* 8 (1/3): 51–57.

Pilato G. & Binda M.G. 2010. Definition of families, subfamilies, genera and subgenera of the Eutardigrada, and keys to their identification. *Zootaxa* 2404 (1): 1–54. https://doi.org/10.11646/zootaxa.2404.1.1

Pilato G. & Lisi O. 2006. *Macrobiotus rigidus* sp. nov., new species of eutardigrade from New Zealand. *Zootaxa* 1109: 49–55. https://doi.org/10.11646/zootaxa.1109.1.5

Pilato G., Napolitano A. & Manicardi E. 2000. The specific value of *Macrobiotus coronatus* de Barros, 1942, and description of two new species of the *harmsworthi* group (Eutardigrada). *Bolletino dell'Accademia gioenia di Scienze naturali, Catania* 33: 103–120

Pilato G., Sabella G. & Lisi O. 2014. Two new tardigrade species from Sicily. *Zootaxa* 3754 (2): 173–184. https://doi.org/10.11646/zootaxa.3754.2.6

Pleijel F., Jondelius U., Norlinder E., Nygren A., Oxelman B., Schander C., Sundberg P. & Thollesson M. 2008. Phylogenies without roots? A plea for the use of vouchers in molecular phylogenetic studies. *Molecular Phylogenetics and Evolution* 48 (1): 369–371. https://doi.org/10.1016/j.ympev.2008.03.024

Rambaut A., Drummond A.J., Xie D., Baele G. & Suchard M.A. 2018. Posterior summarisation in Bayesian phylogenetics using Tracer 1.7. *Systematic Biology* 67 (5): 901–904. https://doi.org/10.1093/sysbi o/syy032

Ronquist F. & Huelsenbeck J.P. 2003. MrBayes 3: Bayesian phylogenetic inference under mixed models. *Bioinformatics* 19: 1572–1574. https://doi.org/10.1093/bioinformatics/btg180

Roszkowska M., Stec D., Gawlak M. & Kaczmarek Ł. 2018. An integrative description of a new tardigrade species *Mesobiotus romani* sp. nov (Macrobiotidae; *harmsworthi* group) from the Ecuadorian Pacific coast. *Zootaxa* 4450 (5): 550–564. https://doi.org/10.11646/zootaxa.4450.5.2

Short K.A., Sands C.J., McInnes S.J., Pisani D., Stevens M.I. & Convey P. 2022. An ancient, Antarctic-specific species complex: large divergences between multiple Antarctic lineages of the tardigrade genus *Mesobiotus*. *Molecular Phylogenetics and Evolution* 170: 107429. https://doi.org/10.1016/j.ympev.2022.107429

Stec D. 2019. *Mesobiotus datanlanicus* sp. nov., a new tardigrade species (Macrobiotidae: *Mesobiotus harmsworthi* group) from Lâm Đồng Province in Vietnam. *Zootaxa* 4679 (1): 164–180. https://doi.org/10.11646/zootaxa.4679.1.10

Stec D. 2021. Integrative descriptions of two new *Mesobiotus* species (Tardigrada, Eutardigrada, Macrobiotidae) from Vietnam. *Diversity* 13: 605. https://doi.org/10.3390/d13110605

Stec D. 2022. An integrative description of two new *Mesobiotus* species (Tardigrada: Eutardigrada: Macrobiotidae) with updated genus phylogeny. *Zoological Studies* 61: 85. https://doi.org/10.3390/d13110605

Stec D. & Kristensen R.M. 2017. An integrative description of *Mesobiotus ethiopicus* sp. nov. (Tardigrada: Eutardigrada: Parachela: Macrobiotidae: *harmsworthi* group) from the Northern Afrotropic region. *Turkish Journal of Zoology* 41: 800–811. https://doi.org/10.3906/zoo-1701-47

Stec D., Gąsiorek P., Morek W., Kosztyła P., Zawierucha K., Michno K., Kaczmarek Ł., Prokop Z.M. & Michalczyk Ł. 2016. Estimating optimal sample size for tardigrade morphometry. *Zoological Journal of the Linnean Society* 178 (4): 776–784. https://doi.org/10.1111/zoj.12404

Stec D., Roszkowska M., Kaczmarek Ł. & Michalczyk Ł. 2018. An integrative description of a population of *Mesobiotus radiatus* (Pilato, Binda and Catanzaro, 1991) from Kenya. *Turkish Journal of Zoology* 42: 523–540. https://doi.org/10.3906/zoo-1802-43

Stec D., Kristensen R.M. & Michalczyk Ł. 2020a. An integrative description of *Minibiotus ioculator* sp. nov. from the Republic of South Africa with notes on *Minibiotus pentannulatus* Londoño *et al*., 2017 (Tardigrada: Macrobiotidae). *Zoologischer Anzeiger* 286: 117–134. https://doi.org/10.1016/j.jcz.2020.03.007

Stec D., Krzywański Ł., Zawierucha K. & Michalczyk Ł. 2020b. Untangling systematics of the *Paramacrobiotus areolatus* species complex by an integrative redescription of the nominal species for the group, with multilocus phylogeny and species delineation in the genus *Paramacrobiotus. Zoological Journal of the Linnean Society* 188: 694–716. https://doi.org/10.1093/zoolinnean/zlz163

Stec D., Krzywański Ł., Arakawa K. & Michalczyk Ł. 2020c. A new redescription of *Richtersius coronifer*, supported by transcriptome, provides resources for describing concealed species diversity within the monotypic genus *Richtersius* (Eutardigrada). *Zoological Letters* 6: 2. https://doi.org/10.1186/s40851-020-0154-y

Stec D., Vecchi M., Calhim S. & Michalczyk Ł. 2021a. New multilocus phylogeny reorganises the family Macrobiotidae (Eutardigrada) and unveils complex morphological evolution of the *Macrobiotus hufelandi* group. *Molecular Phylogenetics and Evolution* 160: 106987. https://doi.org/10.1016/j.ympev.2020.106987

Stec D., Vecchi M., Dudziak M., Bartels P.J., Calhim S. & Michalczyk Ł. 2021b. Integrative taxonomy resolves species identities within the *Macrobiotus pallarii* complex (Eutardigrada: Macrobiotidae). *Zoological Letters* 7: 9. https://doi.org/10.1186/s40851-021-00176-w

Stec D., Vončina K., Kristensen R.M. & Michalczyk Ł. 2022. The *Macrobiotus ariekammensis* species complex provides evidence for parallel evolution of claw elongation in macrobiotid tardigrades. *Zoological Journal of the Linnean Society* 195: 1067–1099. https://doi.org/10.1093/zoolinnean/zlab101

Tamura K., Stecher G. & Kumar S. 2021. MEGA11: Molecular Evolutionary Genetics Analysis version 11. *Molecular Biology and Evolution* 38: 3022–3027. https://doi.org/10.1093/molbev/msab120

Tumanov D.V. 2018a. *Hypsibius vaskelae*, a new species of Tardigrada (Eutardigrada, Hypsibiidae) from Russia. *Zootaxa* 4399 (3): 434. https://doi.org/10.11646/zootaxa.4399.3.12

Tumanov D.V. 2018b. *Mesobiotus nikolaevae* sp. n. (Eutardigrada: Macrobiotidae), a new species of Tardigrada from Croatia. *Invertebrate Zoology* 15 (4): 402–419. https://doi.org/10.15298/invertzool.15.4.08

Tumanov D.V. 2020a. Integrative description of *Mesobiotus anastasiae* sp. nov. (Eutardigrada, Macrobiotoidea) and first record of *Lobohalacarus* (Chelicerata, Trombidiformes) from the Republic of South Africa. *European Journal of Taxonomy* 726: 102–132. https://doi.org/10.5852/ejt.2020.726.1179

Tumanov D.V. 2020b. Integrative redescription of *Hypsibius pallidoides* Pilato *et al*., 2011 (Eutardigrada: Hypsibioidea) with the erection of a new genus and discussion on the phylogeny of Hypsibiidae. *European Journal of Taxonomy* 681: 1–37. https://doi.org/10.5852/ejt.2020.681

Tumanov D.V. & Pilato G. 2019. A new species of Eutardigrade (Macrobiotidae) from New Zealand. *Zootaxa* 4603 (3): 537–548. https://doi.org/10.11646/zootaxa.4603.3.6

Tumanov D.V., Androsova E.D., Avdeeva G.S. & Leontev A.A. 2022. First faunistic investigation of semiterrestrial tardigrade fauna of North-West Russia using the method of DNA barcoding. *Invertebrate Zoology* 19 (4): 452–474. https://doi.org/10.15298/invertzool.19.4.08

Utsugi K. 1988. Tardigrades in Hokkaido area. *Zoological Science* 5: 1335.

Vecchi M., Cesari M., Bertolani R., Jönsson K.I., Rebecchi L. & Guidetti R. 2016. Integrative systematic studies on tardigrades from Antarctica identify new genera and new species within Macrobiotoidea and Echiniscoidea. *Invertebrate Systematics* 30 (4): 303–322. https://doi.org/10.1071/IS15033

Vecchi M., McDaniel J.L., Chartrain J., Vuori T., Walsh E.J. & Calhim S. 2023. Morphology, phylogenetic position, and mating behaviour of a new *Mesobiotus* (Tardigrada) species from a rock pool in the Socorro Box Canyon (New Mexico, USA). *The European Zoological Journal* 90 (2): 708–725. https://doi.org/10.1080/24750263.2023.2263033

Vecchi M., Stec D., Rebecchi L., Michalczyk Ł. & Calhim S. 2024. Ecology explains anhydrobiotic performance across tardigrades, but the shared evolutionary history matters more. *Journal of Animal Ecology* 93: 307–318. https://doi.org/10.1111/1365-2656.14031

Manuscript received: 11 February 2024
Manuscript accepted: 8 April 2024
Published on: 30 July 2024
Topic editor: Magalie Castelin
Section editor: Daniel Stec
Desk editor: Pepe Fernández

Ciencias Naturales-CSIC, Madrid, Spain; Leibniz Institute for the Analysis of Biodiversity Change, Bonn – Hamburg, Germany; National Museum of the Czech Republic, Prague, Czech Republic; The Steinhardt Museum of Natural History, Tel Aviv, Israël.

Supplementary files

Supp. file 1. Primers and PCR programs used for amplification of four DNA fragments sequenced in the study. https://doi.org/10.5852/ejt.2024.947.2619.12005

Supp. file 2. Final alignment used for the phylogenetic analyses.
https://doi.org/10.5852/ejt.2024.947.2619.12007

Supp. file 3. Results of the selection of substitution model for redefined partitions.
https://doi.org/10.5852/ejt.2024.947.2619.12009

Supp. file 4. Measurements of animals and eggs of *Mesobiotus efa* sp. nov.
https://doi.org/10.5852/ejt.2024.947.2619.12011

Supp. file 5. Measurements of animals and eggs of *Mesobiotus vulpinus* sp. nov.
https://doi.org/10.5852/ejt.2024.947.2619.12013

Supp. file 6. Matrices of *p*-distances for species of *Mesobiotus* Vecchi, Cesari, Bertolani, Jönsson, Rebecchi & Guidetti, 2016. https://doi.org/10.5852/ejt.2024.947.2619.12015